*remote sensing*

MDPI

*Article*

# Intercomparison of AVHRR GIMMS3g, Terra MODIS, and SPOT-VGT NDVI Products over the Mongolian Plateau

**Yongqing Bai [1,2], Yaping Yang [1,3,*] and Hou Jiang [1,2]**

1 State Key Laboratory of Resources and Environmental Information System, Institute of Geographic Sciences and Natural Resources Research, Chinese Academy of Sciences, Beijing 100101, China
2 University of Chinese Academy of Sciences, Beijing 100049, China
3 Jiangsu Center for Collaborative Innovation in Geographical Information Resource Development and Application, Nanjing 210023, China
* Correspondence: yangyp@igsnrr.ac.cn; Tel.: +86-10-6488-9452

Received: 10 July 2019; Accepted: 27 August 2019; Published: 29 August 2019


**Abstract:** The rapid development of remote sensing technology has promoted the generation of different vegetation index products, resulting in substantive accomplishment in comprehensive economic development and monitoring of natural environmental changes. The results of scientific experiments based on various vegetation index products are also different with the variation of time and space. In this work, the consistency characteristics among three global normalized difference vegetation index (NDVI) products, namely, GIMMS3g NDVI, MOD13A3 NDVI, and SPOT-VGT NDVI, are intercompared and validated based on Landsat 8 NDVI at biome and regional scale over the Mongolian Plateau (MP) from 2000 to 2014 by decomposing time series datasets. The agreement coefficient (AC) and statistical scores such as Pearson correlation coefficient, root mean square error (RMSE), mean bias error (MBE), and standard deviation (STD) are used to evaluate the consistency between three NDVI datasets. Intercomparison results reveal that GIMMS3g NDVI has the highest values basically over the MP, while SPOT-VGT NDVI has the lowest values. The spatial distribution of AC values between various NDVI products indicates that the three NDVI datasets are highly consistent with each other in the northern regions of the MP, and MOD13A3 NDVI and SPOT-VGT NDVI have better consistency in expressing vegetation cover and change trends due to the highest proportions of pixels with AC values greater than 0.6. However, the trend components of decomposed NDVI sequences show that SPOT-VGT NDVI values are about 0.02 lower than the other two datasets in the whole variation periods. The zonal characteristics show that GIMMS3g NDVI in January 2013 is significantly higher than those of the other two datasets. However, in July 2013, the three datasets are remarkably consistent because of the greater vegetation coverage. Consistency validation results show that values of SPOT-VGT NDVI agree more with Landsat 8 NDVI than GIMMS3g NDVI and MOD13A3 NDVI, and the consistencies in the northeast of the MP are higher than northwest regions.

**Keywords:** NDVI consistency assessment; Mongolian Plateau; intercomparison; consistency validation; terrestrial ecoregion

## 1. Introduction

Vegetation is a crucial component of the terrestrial surface system, which plays a vital role as a regulator in global and regional biochemical cycle, water and energy balance, and climate change [1–3]. Vegetation spectral characteristics show obvious differences in the adjacent spectral space. Vegetation index (VI), computed by a specific combination of different bands, can qualitatively or quantitatively characterize vegetation status on the land surface [1,4,5]. After nearly 40 years of

development, more than 40 vegetation indices have been defined [6] and have been widely used in modeling and monitoring global and regional climate change [1,7–12], identifying vegetation phenology [13–19], investigating the desert boundaries [20], detecting desertification changes [21], classifying and surveying land use/land cover [22–26], and assessing natural disasters such as drought and fire risk [3,27–30]. With the rapid development of remote sensing technology, the study of VI has also changed from pure numerical calculation to factor analysis. Meanwhile, many environmental factors such as atmospheric conditions and soil background may produce errors in these indices [31]. The enhanced vegetation index (EVI) and the normalized difference vegetation index (NDVI) are both effective VIs and are widely applied in providing consistent spatial and temporal information regarding global vegetation. EVI provides improved sensitivity in high biomass regions while minimizing soil and atmosphere influences, which is superior to NDVI in characterizing surface vegetation in areas with high vegetation coverage. However, EVI is limited to sensor systems designed with a blue band, in addition to the red and near-infrared bands, making it difficult to generate long-term EVI time series as the NDVI counterpart [32]. Furthermore, topographic effect on the EVI is much more obvious than that of NDVI, especially in areas of rough terrain [31]. Thus, NDVI becomes the most classical VI in practical application with its advantages of simple calculation, high sensitivity of vegetation detection, and better temporal and spatial adaptability. Refs. [33,34], while serious oversaturation in areas with high vegetation cover is the biggest limitation of NDVI [35].

Continuous and consistent VI datasets are the basis and prerequisite for long-term monitoring of land surface vegetation characteristics [12,13,15,36]. At present, many long time series remote sensing-based VI products have been produced, among which the Global Inventory Modeling and Mapping Studies (GIMMS) NDVI, Moderate Resolution Imaging Spectroradiometer (MODIS) NDVI, and Systeme Probatoire d'Observation de la Terre-VEGETATION (SPOT-VGT) NDVI are the longest time series and the most widely used NDVI datasets [36–39]. As the vital database to characterize the vegetation distribution and dynamic variation monitoring over long period of time, these NDVI datasets have supported massive scientific researches [40–46]. However, because of the different sensor platforms, data processing methods, precision control flow, and distinctive spatial and temporal resolutions, diverse NDVI products reflect different fractional vegetation cover and variation trends, even in the same study region. Beck [47] compared four AVHRR-derived NDVI and MODIS NDVI datasets in detail at a global scale. The results showed that the MODIS NDVI performed better than any AVHRR NDVI datasets in consistency evaluation against Landsat-based NDVI, but GIMMS NDVI could effectively reflect the dynamic changes of vegetation in the four AVHRR NDVI datasets. Gallo's [48] research in the United States showed that the values of AVHRR NDVI were very similar to the 16d synthetic values of MODIS NDVI, and that there was a linear relationship between different sensors. The results evinced that it is feasible to use different sensors to establish NDVI time series. Fensholt [49] took MODIS NDVI as a reference and considered that the GIMMS NDVI dataset had poor ability to explain the interannual changes of vegetation in semi-humid regions of Africa. Song's [50] research indicated that MODIS NDVI and SPOT-VGT NDVI in northern Shaanxi Province showed a significant increase trend from 1999 to 2006, while GIMMS NDVI did not change much in the same period. The above studies clarify that the NDVI has obvious spatial heterogeneity, and the impacts of time duration and space environment on different datasets are various. In order to accurately grasp and recognize the real situation of surface vegetation in specified regions, it is necessary to deeply analyze the consistency of spatial and temporal succession of the three NDVI datasets. Also, the comparison could be a reference to reveal the temporal and spatial applicability of each kind of NDVI data.

The Mongolian Plateau (MP) is the core region of the economic corridor between China, Mongolia, and Russia, and the impact of economic development, industrial structure, and human activities from these three countries on the natural environment of the MP varies greatly. The arid–semi-arid climate environment in the MP makes the ecological environment of the region vulnerable and sensitive. Its extensive vegetation coverage is of great significance for the adjustment of local climate change and the improvement of human living environment. Clearly understanding the characteristics and

current situation of vegetation change in the MP plays an important role in decision-making to cope with climate change in temperate regions of the Northern Hemisphere. At present, there are many studies based on a single NDVI dataset in the MP region, but few of them focus on various datasets. Studying the consistency of vegetation index in the MP will have a far-reaching impact on ecological environment protection and regional and global climate change regulation in the region. It can evaluate the applicability of various datasets in vegetation assessment of the MP, and provide data references for subsequent research. Therefore, this study aims to analyze the succession consistency between GIMMS3g NDVI, MOD13A3 NDVI, and SPOT-VGT NDVI of the MP to reveal the differences of three NDVI datasets in spatial and temporal distribution. The objectives of this study are: (1) Analyze the variation characteristics of the three NDVI datasets over the MP in the past 15 years on a monthly scale and uncover their consistency and differences; (2) reveal the spatial heterogeneity of NDVI distribution by introducing the World Wildlife Fund (WWF) terrestrial ecoregion; (3) verify the reliability of the NDVI values of the three datasets using Landsat 8 images. The remainder of this paper is organized as follow: Section 2 presents the study area, datasets, and methodologies. The results, discussions, and conclusions are given in Section 3, Section 4, and Section 5, respectively.

## 2. Materials and Methods

### *2.1. Study Area*

This study was conducted in the MP, covering the whole territory of Mongolia, the Inner Mongolia Autonomous Region (IMAR) of northern China, Tuva Republic, Buryatia Republic, Zabaykalsky Krai, and parts of Irkutsk Oblast of southern Russia (Figure 1), with a total area of about 3.82 million $km^2$. As one of the most important tectonic landform units of the Eurasian continent, and the typical area of the monsoon marginal zone, the MP is affected by the Siberia–Mongolia high atmospheric pressure in winter and East Asian summer monsoon in summer, resulting in a dry and cold climate in winter but rainy and hot climate in summer [51]. Under the combined influences of monsoon and westerly circulation, the MP becomes the most sensitive and typical region in response to East Asia and global climate change. Figure 1 shows the digital elevation model (DEM) of the MP based on global SRTM data (http://srtm.csi.cgiar.org/srtmdata/). The altitude of the study area ranges from 86 to 4203 m, in which the western and southern parts are mountainous with large relief, while the eastern parts and the Baikal Lake basin have lower elevation and relatively flat terrain. The MP has a temperate continental climate with an average annual rainfall of about 200 mm. It is one of the cold areas in the Asian continent because of its long cold winter; the lowest temperature can reach −40 °C, often accompanied by heavy snowstorms. However, in summer, the highest temperature can reach 35 °C with abundant light and strong ultraviolet radiation [52,53]. Meanwhile, the MP has a very large temperature difference between day and night in summer. The MP is a transboundary region, covered by various types of vegetation and land use because of diverse climate, economic mode, and farming methods. Forest is concentrated in the relatively flat area of the northern MP, especially in the Russian region and the Hinggan Mountains forest area of the northern IMAR of China. Grassland and arable land are the main land cover types in the southeastern part of the IMAR and the northern and eastern parts of Mongolia. There are large areas of desert and bare land in western and southern parts of Mongolia and the western part of the IMAR, in which the vegetation coverage is extremely low and the ecological environment is extremely fragile. The large water bodies in the MP are Lake Baikal in Russia (the deepest freshwater lake in the world), Lake Kusugur in Northern Mongolia, Lake Ubsu, Lake Kyrgyz, Lake Hal, Lake Halwusu and Lake Delle in Western Mongolia, Lake Hulun and Lake Buir in Eastern Mongolia and Northern IMAR.

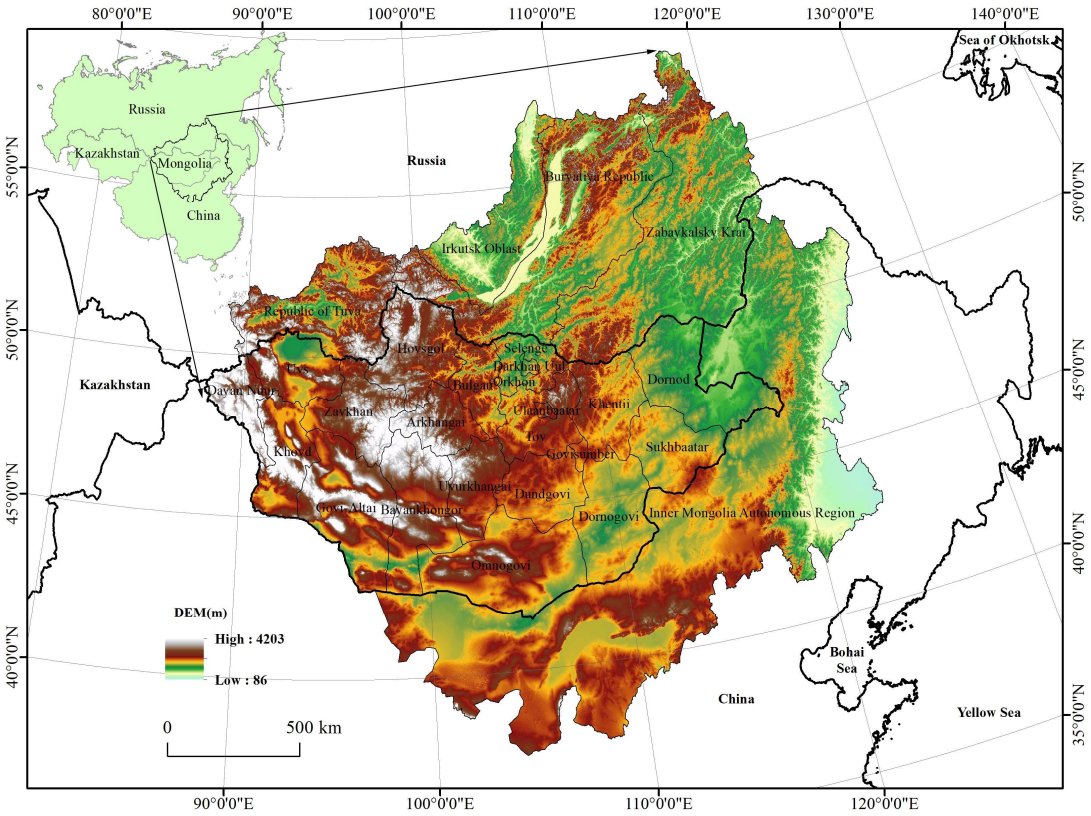


**Figure 1.** Geographic location and elevation of the Mongolian Plateau (MP).

## *2.2. Datasets*

### 2.2.1. NDVI Datasets

Three NDVI products were investigated in this work, namely, GIMMS3g.v1 NDVI, SPOT-VEGETATION-S10 NDVI, and MOD13A3 NDVI. GIMMS NDVI data comprise a long time series global vegetation index dataset based on National Oceanic and Atmospheric Administration (NOAA) meteorological satellites (NOAA 7, 9, 11, 14, 16, 17 and 18). The satellites were launched by National Aeronautics and Space Administration (NASA) in November 2003, equipped with an Advanced Very High Resolution Radiometer (AVHRR) sensor, which provides necessary data guarantee for monitoring multi-year vegetation cover change. Amongst the long-term AVHRR-based datasets analyzed, the GIMMS3g is found to have the highest temporal consistency and, at present state, is the most appropriate choice for NDVI trend analysis [12,13,26,36–41]. The GIMMS3g.v1 NDVI dataset was collected from the Ecological Forecasting Lab at NASA Ames Research Center (https://ecocast.arc.nasa.gov/data/pub/gimms/) in netcdf4 format from July 1981 to December 2015 with a spatial resolution of 1/12 degree and a temporal resolution of 15 days. The SPOT-VGT NDVI dataset is derived from the VEGETATION sensor sponsored by the European Union Commission. The VEGETATION sensor was lunched on board SPOT-4 in March 1998 and has been used for global vegetation cover observations since April 1998. The SPOT VEGETATION-S10 NDVI dataset was downloaded from the Flemish Institute for Technological Research (https://www.vito-eodata.be/) in HDF4 format from April 1998 to May 2015 with a spatial resolution of 950.469 m and a temporal resolution of 10 days. The MOD13A3 NDVI dataset was obtained from the NASA MOD13A3.006 product via the Terra satellite platform at a spatial resolution of 926.625 m and a temporal resolution of 1 month, and 11 scene (h23v03, h23v04, h24v03, h24v04, h25v03, h25v04, h25v05, h26v03, h26v04, h26v05, and h27v04) MODIS images were collected from February 2000 to November 2018 over the MP (https://earthdata.nasa.gov/). The systematic parameters of the three NDVI products are shown in Table 1. Because of the different time ranges of the three NDVI datasets, we chose the

intersection of the three periods from February 2000 to May 2014 to carry out the research. Referring to the synthesis method of the MOD13A3 monthly dataset, the 15-day GIMMS3g NDVI and 10-day SPOT-VGT NDVI were averaged to monthly NDVI values to facilitate comparative analysis of their consistencies. Moreover, the MOD13A3 NDVI and SPOT-VGT NDVI products were resampled to the resolution of the GIMMS3g NDVI to satisfy the spatial correspondence of surface features in the three NDVI datasets. The water bodies in the research area are masked out with the Version 6 MOD44W dataset, which is derived using a decision tree classifier trained with MODIS data to provide a global map of surface water at 250 m spatial resolution [54] (https://e4ftl01.cr.usgs.gov/MOLT/MOD44W.006/).

**Table 1.** Comparison of systematic parameters of three normalized difference vegetation index (NDVI) products.

| NDVI Products | GIMMS3g NDVI | MOD13A3 NDVI | SPOT-VGT NDVI |
|---|---|---|---|
| Satellite | NOAA-16<br>NOAA-17<br>NOAA-18 | TERRA | SPOT-4<br>SPOT-5 |
| Sensor | AVHRR | MODIS | VEGETATION |
| Spectral range | 0.55–12.5 μm | 0.4–14.4 μm | 0.43–1.75 μm |
| Number of bands | 5 | 36 | 5 |
| Bandwidth | RED: 0.585–0.680 μm<br>NIR: 0.730–0.980 μm | RED: 0.620–0.670 μm<br>NIR: 0.841–0.876 μm | RED: 0.61–0.68 μm<br>NIR: 0.79–0.89 μm |
| Radiometric resolution | 8 bits | 12 bits | 8 bits |
| Ground resolution | Primary image: 1.1 km<br>GIMMS3g.v1 NVDI: 1/12 degree | Primary image: 250 m<br>MOD13A3 NDVI: 926.625 m | Primary image: 1.15 km<br>SPOT-VGT NDVI: 950.469 m |
| Temporal resolution | 15 days | 1 month | 10 days |
| Swath width | 2800 km | 2330 km | 60 km |
| Frequency of visit | 0.5 day | 16 days | 26 days |
| Overpass time | 10:15<br>14:00 | 10:35 | 10:30 |
| Resampling method used in this work | —— | Bilinear | Bilinear |
| Temporal compositing method used in this work | Average of two 15-day images | Weighted temporal average of MOD13A2 images | Average of three 10-day images |

#### 2.2.2. Land Cover

The land cover dataset used in this work was collected from the ESA GlobCover 2009 (https://www.osgeo.cn/map/mr8a8). The GlobCover 2009 dataset was jointly completed by the European Space Agency (ESA), United Nations Environment Programme (UNEP), Food and Agriculture Organization (FAO), the Joint Research Centre (JRC) of the European Commission, the International Geosphere-Biosphere Programme (IGBP), and the Global Observation of Forest Cover and Land Dynamics (GOFC-GOLD) [55]. The spatial resolution of GlobCover is 300 m, and different ecoregions are separately extracted by hierarchical classification method. The Land Cover Classification System (LCCS) was used to classify the global land surface into 23 land cover types [56]. Figure 2 shows the land cover of the MP based on the ESA GlobCover 2009.

#### 2.2.3. Terrestrial Ecoregions

The global terrestrial ecoregions dataset used in this work was collected from the WWF website (https://www.worldwildlife.org/). According to the definition from WWF, the terrestrial ecoregions are relatively large units of land or water containing a distinct assemblage of natural communities sharing a large majority of species, dynamics, and environmental conditions [57]. There are 867 terrestrial ecoregions in the world, classified into 14 different biomes such as forests, grasslands, or deserts. By extract with the boundary of the MP, a total of 23 terrestrial ecoregions classified into eight biomes

occur in the study region (Figure 3). In this work, the biome distribution was used to evaluate the consistency of the three NDVI datasets by zonal analysis.

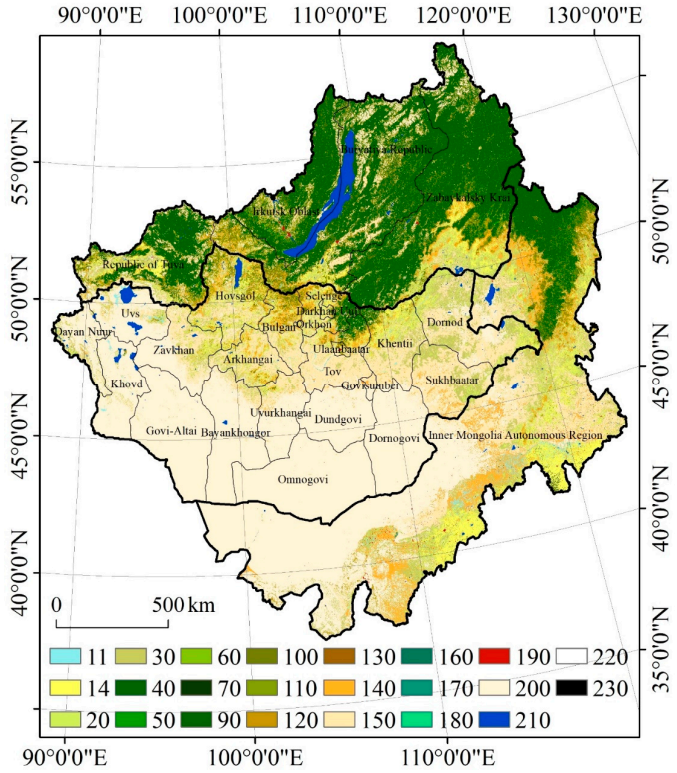


**Figure 2.** Land cover map of the MP based on the ESA GlobCover 2009. The numbers in the legend represent different types of land cover, corresponding to the land cover code in the Table 2.

**Table 2.** Classification of GlobCover 2009 land cover types [56].

| Land Cover Codes | Description of Various Land Cover Types |
|---|---|
| 11 | Post-flooding or irrigated croplands (or aquatic) |
| 14 | Rainfed croplands |
| 20 | Mosaic cropland (50–70%)/vegetation (grassland/shrubland/forest) (20–50%) |
| 30 | Mosaic vegetation (grassland/shrubland/forest) (50–70%)/cropland (20–50%) |
| 40 | Closed to open (>15%) broadleaved evergreen or semi-deciduous forest (>5 m) |
| 50 | Closed (>40%) broadleaved deciduous forest (>5 m) |
| 60 | Open (15–40%) broadleaved deciduous forest/woodland (>5 m) |
| 70 | Closed (>40%) needleleaved evergreen forest (>5 m) |
| 90 | Open (15–40%) needleleaved deciduous or evergreen forest (>5 m) |
| 100 | Closed to open (>15%) mixed broadleaved and needleleaved forest (>5 m) |
| 110 | Mosaic forest or shrubland (50–70%)/grassland (20–50%) |
| 120 | Mosaic grassland (50–70%)/forest or shrubland (20–50%) |
| 130 | Closed to open (>15%) (broadleaved or needleleaved, evergreen or deciduous) shrubland (<5 m) |
| 140 | Closed to open (>15%) herbaceous vegetation (grassland, savannas, or lichens/mosses) |
| 150 | Sparse (<15%) vegetation |
| 160 | Closed to open (>15%) broadleaved forest regularly flooded (semi-permanently or temporarily)—fresh or brackish water |
| 170 | Closed (>40%) broadleaved forest or shrubland permanently flooded—saline or brackish water |
| 180 | Closed to open (>15%) grassland or woody vegetation on regularly flooded or waterlogged soil—fresh, brackish, or saline water |
| 190 | Artificial surfaces and associated areas (urban areas >50%) |
| 200 | Bare areas |
| 210 | Water bodies |
| 220 | Permanent snow and ice |
| 230 | No data (burnt areas, clouds, . . . ) |

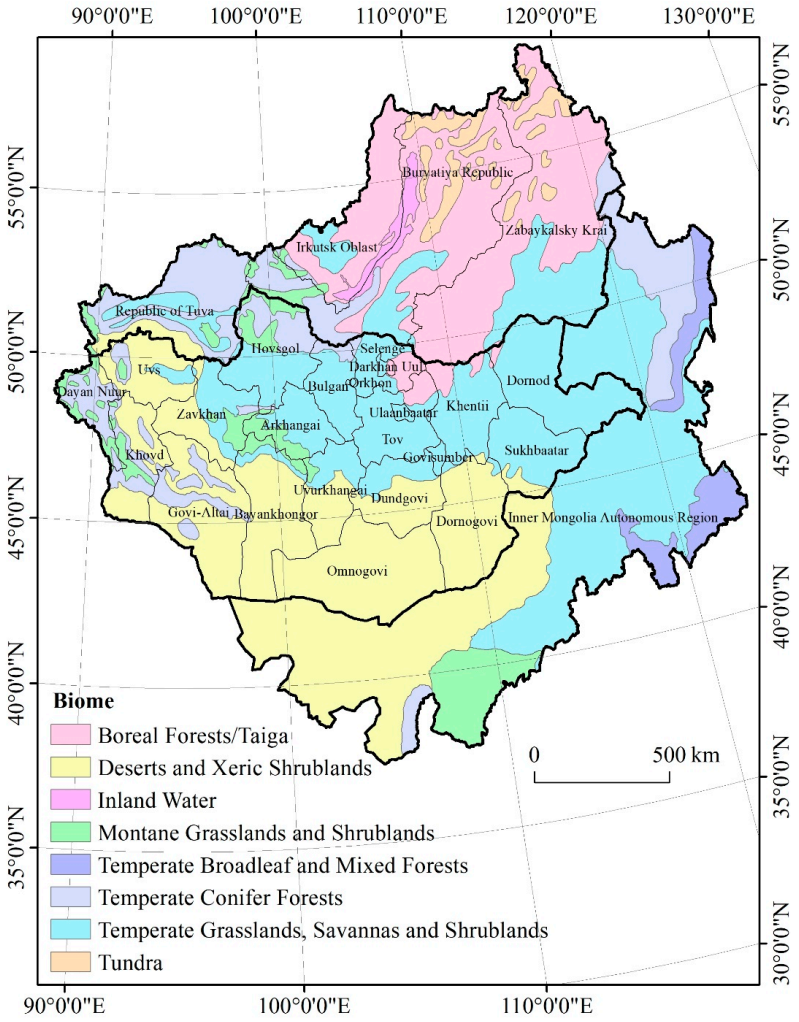


**Figure 3.** Biome distribution of the MP based on the World Wildlife Fund (WWF) terrestrial ecoregion map.

### 2.2.4. The Landsat Image

By amassing information of land surface changes for more than 40 years, the Landsat program have provided decision makers with integral information about the world's food, forests, water, and how these and other land resources are being used. Landsat 8, lunched in February 2013, has been widely used in forest fire monitoring, land use and land cover change analysis, water and forest resources mapping, crops monitoring, disaster risk mapping, and so on [58]. In this work, Landsat 8 OLI/TIRS images were used to compute the NDVI as reference value to verify the agreement of GIMMS3g NDVI, MOD13A3 NDVI, and SPOT-VGT NDVI. There were 35 Landsat 8 Images located in the MP, which were download from the United States Geological Survey (USGS) (https://earthexplorer.usgs.gov/) covering a period from August 2013 to May 2014. In order to effectively utilize the rich spectral information of the Landsat 8 images, the radiometric calibration tool in the ENVI software was used to convert the DN value of original image to spectral reflectance. Then, the Fast Line-of-sight Atmospheric Analysis of Spectral Hypercubes (FLAASH) atmospheric correction model embedded in the ENVI software was applied for atmospheric correction to further remove atmospheric interference of the Landsat 8 images. After radiometric calibration and atmospheric correction, the red and near-infrared bands were used to compute the NDVI value of corresponding regions of Landsat images pixel-by-pixel, using the following formula [59]:

$$NDVI_{Landsat} = \frac{band_{NIR} - band_{RED}}{band_{NIR} + band_{RED}} \quad (1)$$

where $band_{NIR}$ is the near-infrared band of the Landsat images (band 5 in Landsat 8 images), and $band_{RED}$ is the red band of the Landsat images (band 4 in Landsat 8 images).

### *2.3. Methods*

#### 2.3.1. Agreement Coefficient

For objectively assessing the agreement of the data derived from various sources, the agreement coefficient (AC) was employed to evaluate the consistency to compare different images. Compared with traditional statistical methods, including Pearson correlation coefficient ($r$), coefficient of determination ($r^2$), mean absolute error (MAE), and root mean square error (RMSE), AC is capable of quantifying actual differences between different datasets and separating systematic and unsystematic errors [60]. The AC is defined as follows:

$$\mathrm{AC} = 1 - \frac{\sum_{i=1}^{n}(X_i - Y_i)^2}{\sum_{i=1}^{n}\left(\left|\overline{X} - \overline{Y}\right| + \left|X_i - \overline{X}\right|\right)\left(\left|\overline{X} - \overline{Y}\right| + \left|Y_i - \overline{Y}\right|\right)} \quad (2)$$

where $\overline{X}$ and $\overline{Y}$ are the mean values of $X$ and $Y$, respectively. The numerator of the main term of Equation (2) is the sum of square difference (SSD) of $X$ and $Y$, which indicates the degree of disagreement between $X$ and $Y$. The denominator is the sum of potential difference (SPOD) used to standardize SSD. In this work, the AC was computed in Matlab software to evaluate the agreement between the three kinds of NDVI datasets.

#### 2.3.2. Decompose Analysis

Decompose analysis is a crucial means to effectively identify the change pattern, periodicity, and outlier test of long time series data [61,62]. It is usually difficult to visualize an overall variation in NDVI because of its obvious seasonal periodicity. Therefore, decomposing the original data sequence to separate the periodic parts is strongly necessary to analyze the variation regularity of the remaining parts of the data sequence. The Classical Seasonal Decomposition by Moving Averages in R Studio software can efficiently decompose the observed data into three components: Seasonal part, trend part, and random part. The trend component generally describes the gradual variation patterns of the time series datasets. The seasonal component is generally expressed as a periodic change at a special time scale. The residual component is a measure of random variables caused by the observation methodologies, such as the signal-to-noise ratio, and the atmospheric environment, such as clouds and aerosols [63,64]. The function first determines the trend component using a moving average, and removes it from the time series. Then, the seasonal figure is computed by averaging, for each time unit, over all periods. The seasonal figure is then centered. Finally, the error component is determined by removing trend and seasonal figure (recycled as needed) from the original time series [65,66]. There are two types of decompose functions: Additive and multiplicative. As shown in Equation (3), a large number of NDVI values were additively decomposed in this work to reveal its deep-seated change characteristics.

$$Y_t = T_t + S_t + e_t \quad (3)$$

where $Y_t$ is the original observed sequence, $T_t$ means the trend component, $S_t$ means the seasonal component, and $e_t$ means the random component of decomposed data series.

#### 2.3.3. Spatial Statistical Analysis

In this work, Pearson correlation coefficient ($r$), RMSE, MBE, and standard deviation (STD) are used to describe the degree of correlation and the deviation between any two NDVI datasets. The calculation method of those statistical scores can be demonstrated as below.

$$r = \frac{\sum_{i=1}^{n}\left(X_i - \overline{X}\right)\left(Y_i - \overline{Y}\right)}{\sqrt{\sum_{i=1}^{n}\left(X_i - \overline{X}\right)^2 \sum_{i=1}^{n}\left(Y_i - \overline{Y}\right)^2}} \tag{4}$$

$$\mathrm{RMSE} = \sqrt{\frac{1}{n}\sum_{i=1}^{n}(X_i - Y_i)^2} \tag{5}$$

$$\mathrm{MBE} = \frac{1}{n}\sum_{i=1}^{n}(X_i - Y_i) \tag{6}$$

$$\mathrm{STD} = \sqrt{\frac{\sum_{i=1}^{n}\left(X_i - \overline{X}\right)^2}{n-1}} \tag{7}$$

where $X$ and $Y$ represent two kinds of NDVI data; $\overline{X}$ and $\overline{Y}$ are the arithmetic mean of $X$ and $Y$; and $n$ is the number of valid NDVI input data. Pearson correlation coefficient is used to measure the linear relationship between fixed distance variables. The RMSE is used to measure the deviation between the observed value and the true value. It is very sensitive to the large or small errors in a group of measurements. Therefore, the RMSE can well reflect the precision of measurement. MBE is used to describe the degree of difference between two groups of data. STD can objectively and accurately reflect the discreteness of a group of data. A larger STD represents a large difference between most of the values and their average values, and a smaller STD represents that these values are closer to the average value.

## 3. Results

### *3.1. Spatial Consistency Characteristics*

#### 3.1.1. Overall Spatial Patterns

Spatial distribution is a substantial aspect to visualize the zonal regularity of NDVI. Therefore, the AC and MBE are computed pixel-by-pixel between each two datasets of the three NDVIs to reveal their similitudes. Figure 4 shows the spatial distribution of the AC of GIMMS3g NDVI and MOD13A3 NDVI, GIMMS3g NDVI and SPOT-VGT NDVI, and MOD13A3 NDVI and SPOT-VGT NDVI. It was revealed that the three NDVI datasets are highly correlated in most regions. The high AC values mainly distribute in the whole Zabaykalsky Krai, eastern Buryatia Republic, southern Irkutsk Oblast and Republic of Tuva, and northern and eastern Mongolia and the IMAR—more than 70% area of total the MP. The regions with low correlation are mainly desert and sandy areas in southern and western Mongolia and the west of the IMAR. The proportions of pixels with AC values greater than 0.6 for GIMMS3g NDVI and MOD13A3 NDVI, GIMMS3g NDVI and SPOT-VGT NDVI, and MOD13A3 NDVI and SPOT-VGT NDVI are 72.80%, 76.62%, and 80.13%, respectively. Overall, the AC values between MOD13A3 NDVI and SPOT-VGT NDVI are higher than the other NDVI data combinations, which indicates that MOD13A3 NDVI and SPOT-VGT NDVI have better agreement in expressing vegetation cover and change trends in the MP from February 2000 to May 2014.

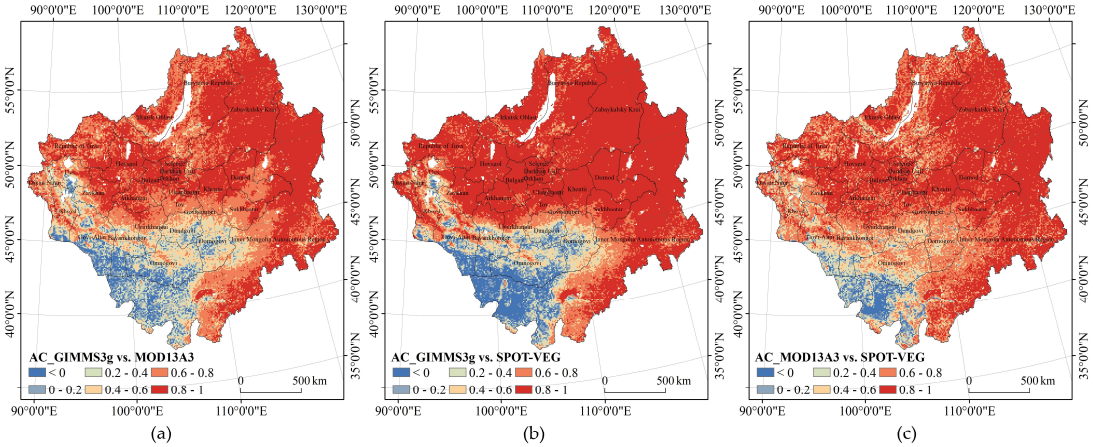


**Figure 4.** Spatial distribution of the agreement coefficient (AC) between (**a**) GIMMS3g NDVI and MOD13A3 NDVI, (**b**) GIMMS3g NDVI and SPOT-VGT NDVI, and (**c**) MOD13A3 NDVI and SPOT-VGT NDVI.

The spatial distributions of MBE between three NDVI datasets are shown in Figure 5. It was found that GIMMS3g NDVI values in 50.46% of pixels widely distributed in the southern MP are smaller than MOD13A3 NDVI values, in which 87% of these pixels with difference below 0.05. Conversely, GIMMS3g NDVI values in 49.54% of pixels intensively distributed in the Lake Baikal basin of the northern MP are larger than MOD13A3 NDVI values, in which 86.77% of these pixels with difference below 0.05. By the same token, GIMMS3g NDVI values in 81.7% of pixels densely distributed in the Russia region and the northeastern IMAR are larger than SPOT-VGT NDVI values, of which 71.18% of these pixels with difference below 0.05. For the third group datasets, MOD13A3 NDVI values in 68.76% of pixels widely distributed in the Russia region and the northeastern IMAR are larger than SPOT-VGT NDVI values, of which 67.51% of these pixels with difference below 0.05. Generally, SPOT-VGT NDVI values are substantially smaller than the values of GIMMS3g NDVI and MOD13A3 NDVI, and GIMMS3g NDVI values are relatively larger than MOD13A3 NDVI values in the northern MP, but just opposite in the southern MP.

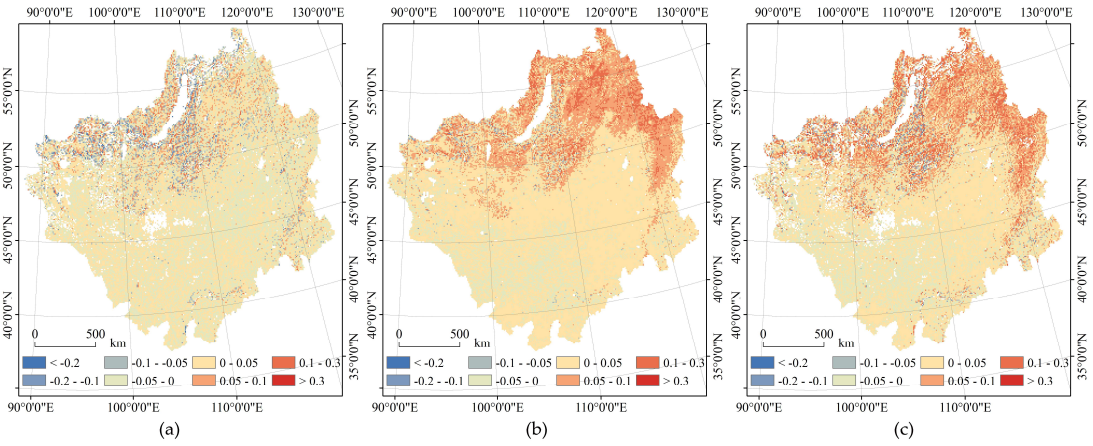


**Figure 5.** Spatial distribution of the mean bias error (MBE) between (**a**) GIMMS3g NDVI and MOD13A3 NDVI, (**b**) GIMMS3g NDVI and SPOT-VGT NDVI, and (**c**) MOD13A3 NDVI and SPOT-VGT NDVI.

### 3.1.2. Spatial Zonality of Terrestrial Ecoregions

Considering the heterogeneity of spatial distribution of NDVI, the consistency and agreement between the three datasets are zonally evaluated over different biomes (regardless of inland water) in the MP. Tables 3 and 4 show the zonally statistical AC and MBE values, respectively.

(1) The biome of montane grasslands and shrublands centrally locate in the southern region of the IMAR and sporadically distribute in Western Mongolia and southwestern regions of Lake Baikal. The main land cover types in this biome are closed to open herbaceous vegetation, including grassland, savannas, and shrublands, according to the ESA GlobCover 2009 map. The largest AC values between GIMMS3g NDVI and SPOT-VGT NDVI in this biome indicate that the correlation between GIMMS3g NDVI and SPOT-VGT NDVI is higher than other combinations in the biome of montane grasslands and shrublands. Meanwhile, the smallest mean MBE values between GIMMS3g NDVI and MOD13A3 NDVI indicate that GIMMS3g NDVI values has a closer average and discrete degree to MOD13A3 NDVI than other combinations in the biome of montane grasslands and shrublands.

(2) The biome of temperate conifer forests mainly locates in the northeastern IMAR, the western border area of Mongolia, the northern part of the Republic of Tuva of Russia, and the Mongolia–Russia border area in the southwest of Lake Baikal. The main types of land cover in the biome are open needleleaved deciduous and evergreen forest. Similarly, the largest AC values between GIMMS3g NDVI and SPOT-VGT NDVI reflect higher consistency of the two datasets in this biome, and the smallest MBE values between GIMMS3g NDVI and MOD13A3 NDVI explain higher proximity in the biome of temperate conifer forests.

(3) The boreal forest/taiga biome, covered with open needleleaved deciduous and evergreen forest, mainly locates in Zabaykalsky Krai, Buryatia Republic, and Irkutsk Oblast in Russia. Because of high evergreen vegetation coverage, the three NDVI datasets have quite high consistency. The largest AC values between GIMMS3g NDVI and SPOT-VGT NDVI in this biome with the smallest STD indicate higher agreement of GIMMS3g NDVI and SPOT-VGT NDVI.

(4) The biome of temperate grasslands, savannas, and shrublands mainly distributes in the north and east parts of Mongolia and the central part of IMAR, which is the largest biome in the study region, with an area exceeding one third of the MP. The land covers of this biome are mainly mosaic vegetation of grasslands, shrublands, forests, and some croplands. The largest AC values are presented between GIMMS3g NDVI and SPOT-VGT NDVI in this biome and the smallest MBE occurs in the combination of GIMMS3g NDVI and MOD13A3 NDVI.

(5) The biome of deserts and xeric shrublands mainly locate in Western and Southern Mongolia, and northwestern IMAR, with dominant land covers of desert and bare areas. Because of very low vegetation coverage, the NDVI values of the three datasets vary differently. Compared with other biomes, the consistency of the three NDVI products in the biome of deserts and xeric shrublands are quite low. The highest average AC value between MOD13A3 NDVI and SPOT-VGTNDVI indicates that the dataset combinations with higher resolution, such as MOD13A3 NDVI and SPOT-VGT NDVI, have higher consistency in desert and bare land in the southwest of the MP.

(6) The biome of temperate broadleaf and mixed forests in the eastern IMAR is mainly covered by mosaic vegetation of shrublands, and needleleaved deciduous and evergreen forests. Just like most biomes in the MP, GIMMS3g NDVI and SPOT-VGT NDVI have the largest AC value and the smallest STD of MBE values in the biome of temperate broadleaf and mixed forests.

(7) Tundra is the smallest biome in the MP, which is mainly covered by intersection of open needleleaved deciduous and evergreen forest and bare areas. Because of near space position with the biome of boreal forest/taiga, the largest AC values similarly occur in the combination of GIMMS3g NDVI and SPOT-VGT NDVI in the biome of tundra. Meanwhile, the negative mean MBE value in the biome of tundra indicates that the values of GIMMS3g NDVI are essentially smaller than MOD13A3 NDVI in the northern region of Zabaykalsky Krai and Buryatia Republic in Russia.

**Table 3.** Zonal statistic results of the AC values between the three NDVI products over the seven biomes of the MP.

| Biome Name | GIMMS3g vs. MOD13A3 | | | | GIMMS3g vs. SPOT-VGT | | | | MOD13A3 vs. SPOT-VG | | | |
|---|---|---|---|---|---|---|---|---|---|---|---|---|
| | Maximum | Minimum | Mean | STD | Maximum | Minimum | Mean | STD | Maximum | Minimum | Mean | STD |
| Montane Grasslands and Shrublands | 0.95 | −0.27 | 0.75 | 0.14 | 0.97 | −1.87 | 0.80 | 0.16 | 0.95 | −1.54 | 0.75 | 0.18 |
| Temperate Conifer Forests | 0.95 | −1.07 | 0.76 | 0.18 | 0.98 | −0.40 | 0.84 | 0.16 | 0.95 | −1.49 | 0.76 | 0.16 |
| Boreal Forests/Taiga | 0.94 | 0.16 | 0.81 | 0.09 | 0.98 | 0.20 | 0.88 | 0.07 | 0.94 | −0.30 | 0.80 | 0.11 |
| Temperate Grasslands, Savannas, and Shrublands | 0.95 | −0.28 | 0.80 | 0.10 | 0.98 | 0.12 | 0.87 | 0.08 | 0.95 | −0.40 | 0.83 | 0.09 |
| Deserts and Xeric Shrublands | 0.95 | −4.64 | 0.28 | 0.46 | 0.97 | −6.18 | 0.17 | 0.70 | 0.96 | −3.81 | 0.46 | 0.44 |
| Temperate Broadleaf and Mixed Forests | 0.96 | 0.14 | 0.86 | 0.07 | 0.98 | 0.51 | 0.89 | 0.06 | 0.96 | −1.09 | 0.86 | 0.10 |
| Tundra | 0.93 | 0.44 | 0.81 | 0.07 | 0.97 | 0.03 | 0.85 | 0.11 | 0.95 | 0.09 | 0.78 | 0.13 |

**Table 4.** Zonal statistic results of the MBE values between the three NDVI products over the seven biomes of the MP.

| Biome Name | GIMMS3g vs. MOD13A3 | | | | GIMMS3g vs. SPOT-VGT | | | | MOD13A3 vs. SPOT-VG | | | |
|---|---|---|---|---|---|---|---|---|---|---|---|---|
| | Maximum | Minimum | Mean | STD | Maximum | Minimum | Mean | STD | Maximum | Minimum | Mean | STD |
| Montane Grasslands and Shrublands | 0.21 | −0.27 | 0.00 | 0.04 | 0.22 | −0.17 | 0.02 | 0.03 | 0.36 | −0.20 | 0.02 | 0.05 |
| Temperate Conifer Forests | 0.31 | −0.34 | 0.00 | 0.06 | 0.23 | −0.25 | 0.05 | 0.05 | 0.40 | −0.37 | 0.05 | 0.07 |
| Boreal Forests/Taiga | 0.29 | −0.32 | 0.01 | 0.06 | 0.22 | −0.21 | 0.07 | 0.04 | 0.43 | −0.28 | 0.06 | 0.07 |
| Temperate Grasslands, Savannas, and Shrublands | 0.25 | −0.30 | 0.00 | 0.03 | 0.17 | −0.15 | 0.02 | 0.03 | 0.30 | −0.31 | 0.02 | 0.04 |
| Deserts and Xeric Shrublands | 0.17 | −0.29 | 0.00 | 0.02 | 0.15 | −0.14 | 0.00 | 0.01 | 0.31 | −0.21 | 0.00 | 0.02 |
| Temperate Broadleaf and Mixed Forests | 0.13 | −0.17 | 0.00 | 0.03 | 0.12 | −0.05 | 0.03 | 0.03 | 0.19 | −0.13 | 0.03 | 0.04 |
| Tundra | 0.18 | −0.21 | -0.01 | 0.06 | 0.20 | −0.11 | 0.06 | 0.04 | 0.30 | −0.26 | 0.07 | 0.06 |

### *3.2. Temporal Variability Characteristics*

#### 3.2.1. Overall Temporal Variations

Trends, seasonal components, and residuals of three long-term NDVI datasets are decomposed in this work. Figure 6a presents the original monthly average NDVI values, and all three NDVI datasets show similar periodic variation. It is suggested that the values of the three NDVI datasets in growing seasons (April to September) are relatively consistent, and the maximum values in June to August gradually increase by nearly 0.05 from 2000 to 2013. However, the lower values of three datasets in non-growing seasons (October to March) vary differently. GIMMS3g NDVI shows sensibly higher values in non-growing season than MOD13A3 NDVI and SPOT-VGT NDVI, and the maximum differences of NDVI values can reach almost 0.04. Meanwhile, SPOT-VGT NDVI remains smallest in all non-growing periods. Figure 6b presents the trend components, in which all three NDVI datasets show an overall upward trend from February 2000 to May 2014, but with a significant decline before April 2000, from 2002 to 2003, from 2008 to 2009, and March to October 2012. The trend curves indicate that MOD13A3 NDVI values have very similar variation trends to SPOT-VGT NDVI values in general, and SPOT-VGT NDVI values are about 0.02 lower than the other two datasets in the whole variation periods. At the same time, the trend curves of GIMMS3g NDVI and MOD13A3 NDVI are much closer. Only in 2000–2001 do the GIMMS3g NDVI show relatively higher values.

Figure 6c shows the seasonal components of the three NDVI datasets. Like the original data series, the three seasonal components have completely similar periodic laws, with only a small range of differences in the amplitudes. The maximum values of SPOT-VGT NDVI in growing seasons are nearly 0.04 higher than the GIMMS3g NDVI and MOD13A3 NDVI, while the latter two NDVI datasets have almost the same peak values. In the same measure, the three seasonal components in non-growing seasons are different to some degree. GIMMS3g NDVI has largest values in non-growing seasons, while MOD13A3 NDVI has the smallest, and the biggest difference between these two datasets is around 0.02. Figure 6d shows the residual of the original data after subtracting the trend and seasonal components. The random components of the three datasets fluctuate around 0 in a range from –0.03 to 0.03, reflecting the distribution of outlines in the original datasets. Compared with MOD13A3 NDVI and SPOT-VGT NDVI, the GIMMS3g NDVI values have the smallest residual fluctuation, indicating that the trend component of GIMMS3g NDVI values is more convincing in experiencing the original datasets.

#### 3.2.2. Temporal Zonality of Terrestrial Ecoregions

Because of the significant spatial heterogeneity of topography and climate factors, the distribution and growth of vegetation also showed obvious zonal characteristics. The seasonal components of three NDVI series were subtracted from the original observed data to get the deseasonalized sequence of datasets. Figure 7 presents the variation of deseasonalized average NDVI values in the seven biomes of the MP. It is shown that the three NDVI datasets in all seven biomes have high consistencies, and essentially share the same or similar peak and valley shape. Overall, the values of SPOT-VGT NDVI are lower than the other two datasets in varying degrees.

(1) Based on Figure 7a, the average values of deseasonalized NDVI in the biome of montane grasslands and shrublands range from 0.11 to 0.25, showing an upward trend of fluctuation. SPOT-VGT NDVI values are about 0.02 lower than the other two NDVI datasets in the whole periods. GIMMS3g NDVI shares very close variation characteristics with MOD13A3 NDVI values, in which the GIMMS3g NDVI values are lower than MOD13A3 NDVI values before 2002, but MOD13A3 NDVI values are higher from 2003.

(2) Figure 7b demonstrates the deseasonalized NDVI values in the biome of temperate conifer forests. The average NDVI values in this biome range from 0.23 to 0.41 with obvious fluctuation in the whole interval, and the difference between SPOT-VGT NDVI values and the other two datasets

in the biome is about 0.04. Compared with MOD13A3 NDVI, the GIMMS3g NDVI values have smaller fluctuation amplitude, which indicates that GIMMS3g NDVI values are less discrete.

(3) As shown in Figure 7c, the NDVI values in the biome of boreal forest/taiga range from 0.23 to 0.53, which is the largest amplitude in all seven biomes. At the same time, the SPOT-VGT NDVI values have the largest differences with GIMMS3g NDVI and MOD13A3 NDVI values in the biome of boreal forest/taiga.

(4) Figure 7d shows the average off-season NDVIs in the biome of temperate grasslands, savannas, and shrublands. As the largest biome in the study region, the differences between SPOT-VGT NDVI values and the other two NDVI datasets in this biome are lower than in the other biomes, and the fluctuation characteristics of the three datasets are relatively consistent, especially in the performance of outliers. In July 2007, all three NDVI data showed abnormally low values in the biome of temperate grasslands, savannas, and shrublands, which can probably be related to the cooling effects caused by the La Niña occurring in 2007.

(5) The average values of deseasonalized NDVI in the biome of deserts and xeric shrublands are shown in Figure 7e. The NDVI values in this biome vary, with the smallest amplitude due to very little vegetation cover. The three datasets come the closest to each other in this biome, which indicates that the three datasets have good consistency in temporal variation in low vegetation coverage area in the southwestern MP.

(6) As shown in Figure 7f, the NDVI values in the biome of temperate broadleaf and mixed forests in the eastern IMAR have an upward trend as a whole. The consistencies of the three datasets are fairly good in this biome, and the differences between SPOT-VGT NDVI values and the other two datasets shrink with the passage of years. In addition, the values of MOD13A3 NDVI are generally higher than GIMMS3g NDVI after 2002 in the biome of temperate broadleaf and mixed forests. However, in December 2012, all three NDVI datasets show abnormally low values in the east of the IMAR, which is likely to be closely related to the extreme low temperature in winter caused by the Arctic Oscillation in 2012.

(7) Figure 7g shows the deseasonalized NDVI values of the biome of tundra, as the smallest biome in the MP, and the variation characteristics of NDVI values in this biome are quite similar to the biome of boreal forest/taiga. The SPOT-VGT NDVI values are significantly lower than the other two NDVI products, and the MOD13A3 NDVI values in this biome have the most obvious fluctuation variation, indicating that it has the highest sensitivity to surface vegetation cover in the biome of tundra in the northern MP.

In order to quantitatively describe the differences among the three NDVI datasets in more detail, STD and slope of 10a of primary linear regression of deseasonalized NDVI values were computed over the seven biomes and the whole MP (Table 5). Overall, the dispersions of MOD13A3 NDVI values and SPOT-VGT NDVI values are larger and more similar than GIMMS3g NDVI values, while GIMMS3g NDVI values are closer to its average. From the perspective of linear regression slope, the three datasets show insignificant growth from 2000 to 2014, in which SPOT-VGT NDVI values have the largest growth rate, while GIMMS3g NDVI values show the smallest increase. On the biome scale, there are larger STD values in the biomes of boreal forests/taiga and tundra, especially for MOD13A3 NDVI. In contrast, the smallest STD values occur in the biomes of deserts and xeric shrublands, montane grasslands and shrublands due to relatively single vegetation cover and insignificant seasonal variation. In terms of linear trend, all positive slope values indicate that the three NDVI datasets show similar insignificant growth trend in the seven biomes. Meanwhile, the MOD13A3 NDVI and SPOT-VGT NDVI have the largest growth of 2.50E-02/10a and 2.83E-02/10a in the biome of temperate broadleaf and mixed forests and the smallest growth of 7.08E-03/10a and 1.03E-02/10a in the biome of deserts and xeric shrublands. However, the GIMMS3g NDVI values show the largest increase at the rate of 9.91E-03/10a in the biome of temperate grasslands, savannas, and shrublands, and the smallest growth of 4.08E-04/10a in the biome of temperate conifer forests.

**Table 5.** Standard deviation (STD) and slope of primary linear regression of deseasonalized NDVI values in the different biomes of the MP.

| Biome Region | GIMMS3g NDVI | | MOD13A3 NDVI | | SPOT-VGT NDVI | |
|---|---|---|---|---|---|---|
| | STD | Slope/10a | STD | Slope/10a | STD | Slope/10a |
| Total MP | 0.0119 | 5.19E-03 | 0.0181 | 1.44E-02 | 0.0174 | 1.95E-02 |
| Montane Grasslands and Shrublands | 0.0130 | 8.72E-03 | 0.0168 | 2.05E-02 | 0.0169 | 2.44E-02 |
| Temperate Conifer Forests | 0.0182 | 4.08E-04 | 0.0230 | 1.57E-02 | 0.0224 | 1.90E-02 |
| Boreal Forests/Taiga | 0.0263 | 2.36E-03 | 0.0360 | 1.50E-02 | 0.0324 | 2.26E-02 |
| Temperate Grasslands, Savannas, and Shrublands | 0.0186 | 9.91E-03 | 0.0287 | 1.79E-02 | 0.0276 | 2.48E-02 |
| Deserts and Xeric Shrublands | 0.0069 | 2.32E-03 | 0.0091 | 7.08E-03 | 0.0113 | 1.03E-02 |
| Temperate Broadleaf and Mixed Forests | 0.0170 | 9.70E-03 | 0.0295 | 2.50E-02 | 0.0287 | 2.83E-02 |
| Tundra | 0.0338 | 1.45E-03 | 0.0343 | 1.77E-02 | 0.0314 | 1.79E-02 |

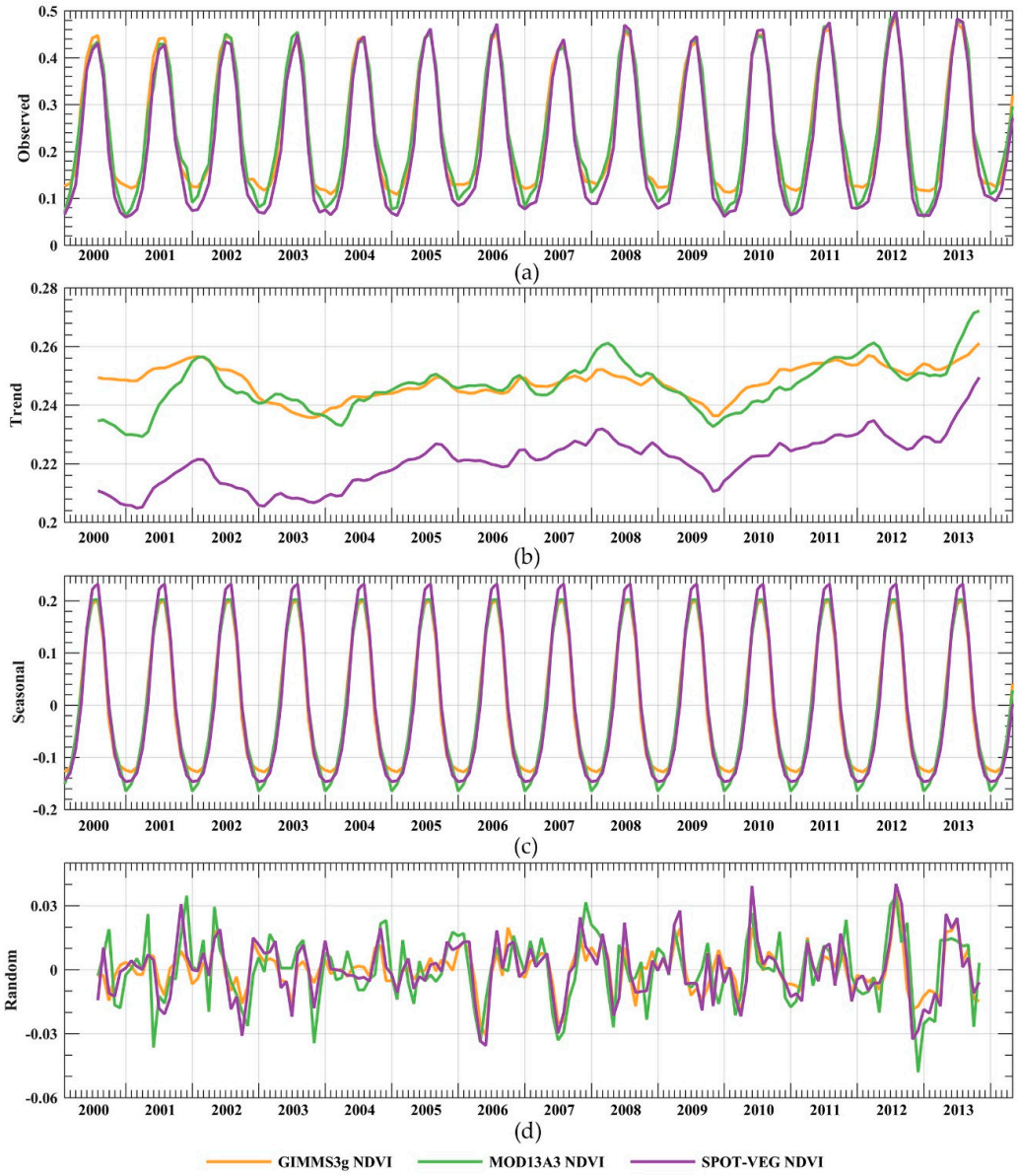


**Figure 6.** Time series of decomposed of GIMMS3g NDVI, MOD13A3 NDVI, and SPOT-VGT NDVI in the MP from February 2000 to May 2014. (**a**) Original observation values, (**b**) variation trends, (**c**) seasonal periodic sequence, and (**d**) the residual parts of three datasets.

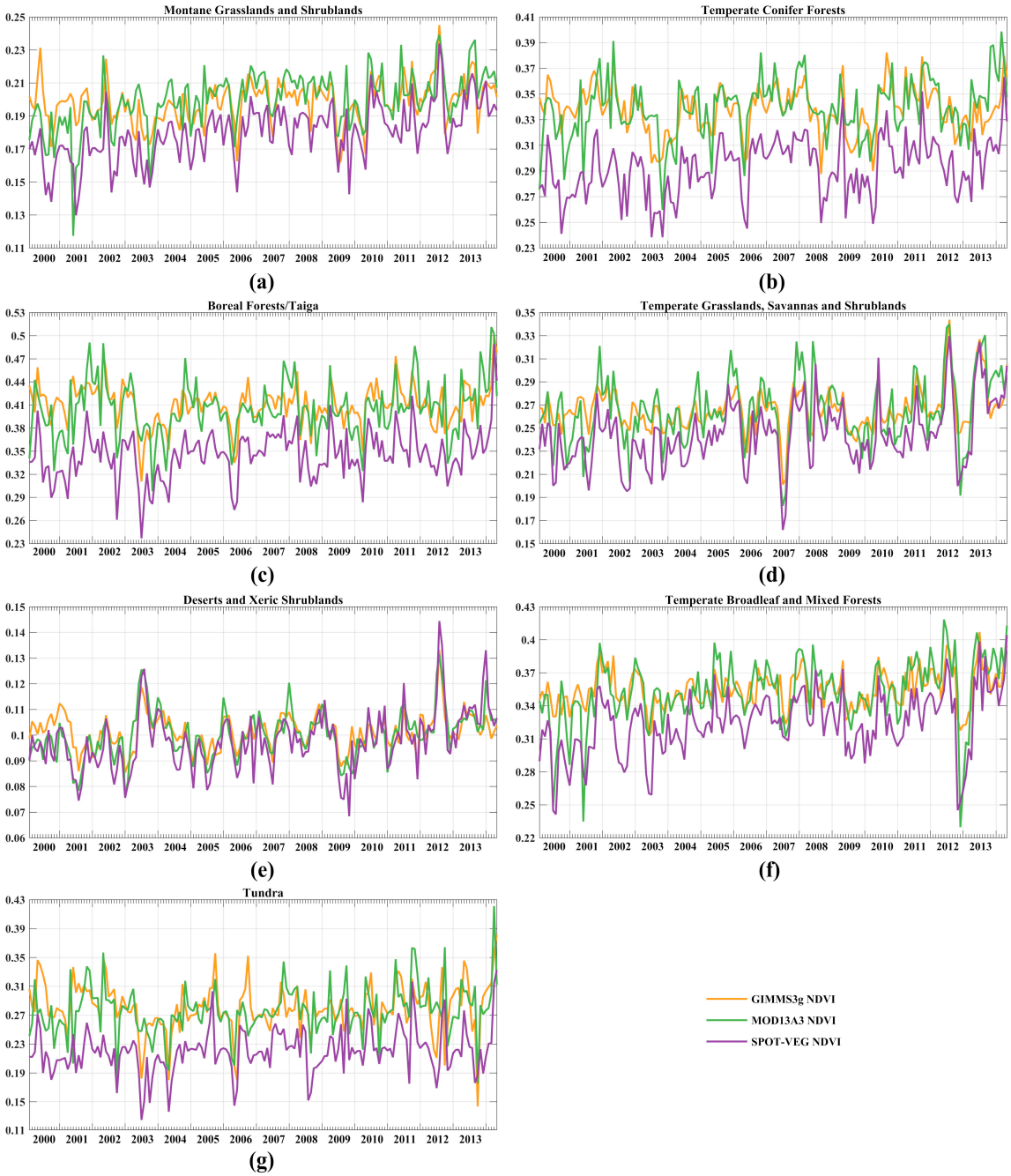


**Figure 7.** Time series of deseasonalized NDVI values in the biomes of (**a**) montane grasslands and shrublands, (**b**) temperate conifer forests, (**c**) boreal forest/taiga, (**d**) temperate grasslands, savannas, and shrublands, (**e**) deserts and xeric shrublands, (**f**) temperate broadleaf and mixed forests and (**g**) tundra in the MP.

## *3.3. Zonal Characteristics of NDVI Variation*

### 3.3.1. Longitudinal and Latitudinal Zonality

The latitude zonality derived by the difference of the incidence angle of sunlight and uneven distribution of solar rays in each latitude on the earth's surface significantly affects climate transition and surface ecological environment evolution. As the vegetation cover of the MP spans forests, grasslands, gobi desert, and agro-pastoral ecotone from north to south [67], the changes of NDVI and its influencing factors have a unique north–south zonal differentiation law. In order to mine the

latitude zonality characteristics of different NDVI datasets in the MP, the average values are computed row-by-row of three gridded NDVI datasets from 37.4°N to 58.4°N. Taking the latest complete year of 2013 as an example, Figure 8 presents the variation of latitude zonality of the three NDVI datasets in January and July 2013. In January 2013, there is a downward trend from the south border of the study region to the center of the MP, reaching a turning point around 46.5°N, and then NDVI values grow rapidly and continuously, reaching a maximum around 52°N. After the peak, the NDVIs show quick decline to the minimum values at 57.42°N. At last, an immediate ascent occurs from the valley to the north border. The values of the three NDVI datasets are highly consistent in the sandy and bare areas south of 40°N. However, GIMMS3g NDVI shows significantly higher values than the other two datasets in the regions north of 40°N, and the gap varies with the latitudes, reaching a relatively large difference around 46.5°N. In the Russia areas north of 50°N, the differences between GIMMS3g NDVI values and the other two NDVI datasets tend to be stable due to the dense vegetation cover. The values of MOD13A3 NDVI and SPOT-VGT NDVI in January 2013 are very close to each other with latitude variation. In July 2013, the average NDVI values of three datasets are highly consistent from south to north. NDVI values grow slowly in the south region of sandy and bare areas, in which a period of abnormally high values appear around 45°N, with the maximum value of NDVI reaching 0.3. From then, the NDVI values increase all the way, reaching the maximum value of 0.8 at the latitude of 53°N, and then decline in a small range to the north, and the SPOT-VGT NDVI values in the north border region are obviously lower than GIMME3g NDVI and MOD13A3 NDVI.

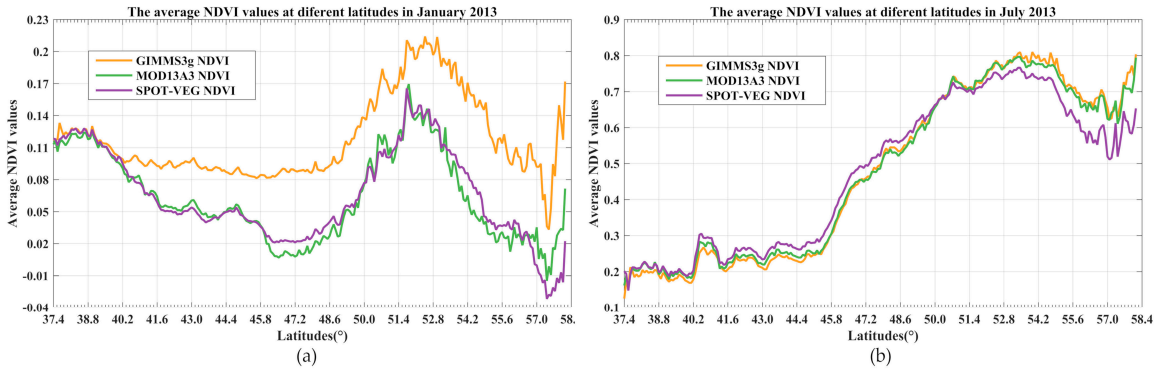


**Figure 8.** Average NDVI values at different latitudes from 37.4°N to 58.4°N in (**a**) January 2013 and (**b**) July 2013.

The longitude zonality derived by the interaction between land and sea notably influences hydrological environment of MP. Similarly, the variation trends of average NDVI values at different longitudes are computed column-by-column of the three gridded NDVI datasets from 87.8°E to 126.1°E in January and July 2013 (Figure 9). In January 2013, the NDVI values show an overall upward trend from the western border to the central MP at 108°E with a small range of downward fluctuation around the longitude of 98°E. Between 108°E and 120°E, there is a symmetrical trend of firstly decreasing and then increasing, and the valley values appear at the longitude of about 115°E. Based on Figure 9a, GIMMS3g NDVI values in the MP are totally higher than the other two datasets, especially in the eastern regions. The values of MOD13A3 NDVI are lower than SPOT-VGT NDVI in the valley periods but higher than SPOT-VGT NDVI in the peak periods. In July 2013, the variation curves of three NDVI datasets are very close to each other, or even partially coincident, showing a trend of rapid decline and then fluctuating rise from west to east. The variation trends of latitudinal and longitudinal zonality of NDVI indicate that evergreen forests are densely distributed in the northeast MP, and there are large areas of grassland or deciduous forests in the central and eastern regions of the MP.

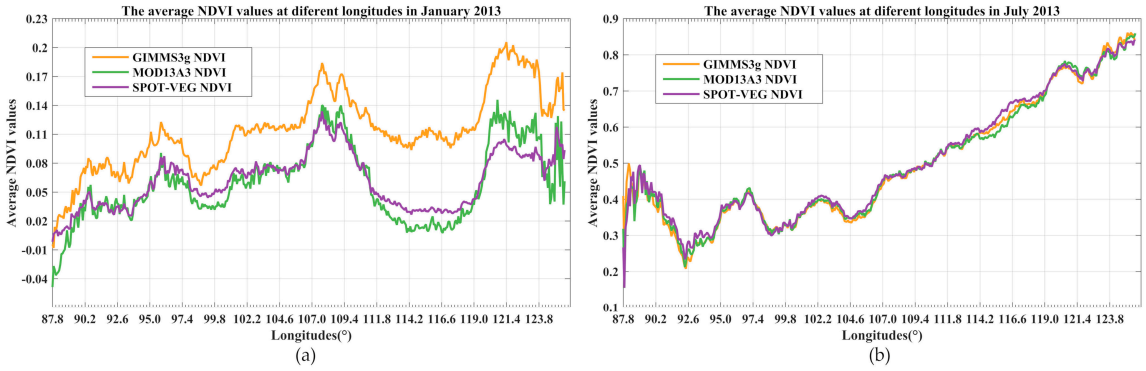


**Figure 9.** Average NDVI values at different longitudes from 87.8°E to 126.1°E in (**a**) January 2013 and (**b**) July 2013.

### 3.3.2. Elevation Effects

The terrain features of the mountain areas affect its climatic characteristics, making the vegetation show significant vertical zonality heterogeneity [68,69]. Revealing the vertical zonal characteristics of vegetation distribution in the MP is a considerable aspect of comparing the three NDVI datasets. Consequently, the average values of NDVI in different elevation ranges in the MP were computed to analyze the vertical zonality of three NDVI datasets. Figure 10 presents the scatter plots and fitting curves of average NDVI values at different elevations in January and July 2013. In January 2013, the average NDVI values show a decreasing trend with the increase of altitude in the MP (Figure 10a). The three NDVI datasets show the same fluctuation characteristics in the altitude range of 200–800 m, and the maximum NDVI values appear at about 500 m of elevation. Overall, the GIMMS3g NDVI values are higher than the other two NDVI datasets at all elevation surfaces, and the difference decreases with the increase of elevation. Furthermore, the values of MOD13A3 NDVI are basically the same as that of SPOT-VGT NDVI in low altitude areas, but in areas above 1800 m, SPOT-VGT NDVI values are gradually larger than MOD13A3 NDVI with the increase of altitude. In July 2013, the average NDVI values increase firstly and then decrease on the whole with the increase of DEM, and the maximum NDVI values distribute at the altitude of 400 m. The areas with NDVI values greater than 0.5 mainly distribute below 1000 m. Based on Figure 10b, the three NDVI datasets show a high degree of uniformity in July 2013. Only in the areas with altitude below 400 m are SPOT-VGT NDVI values slightly higher than the other two datasets.

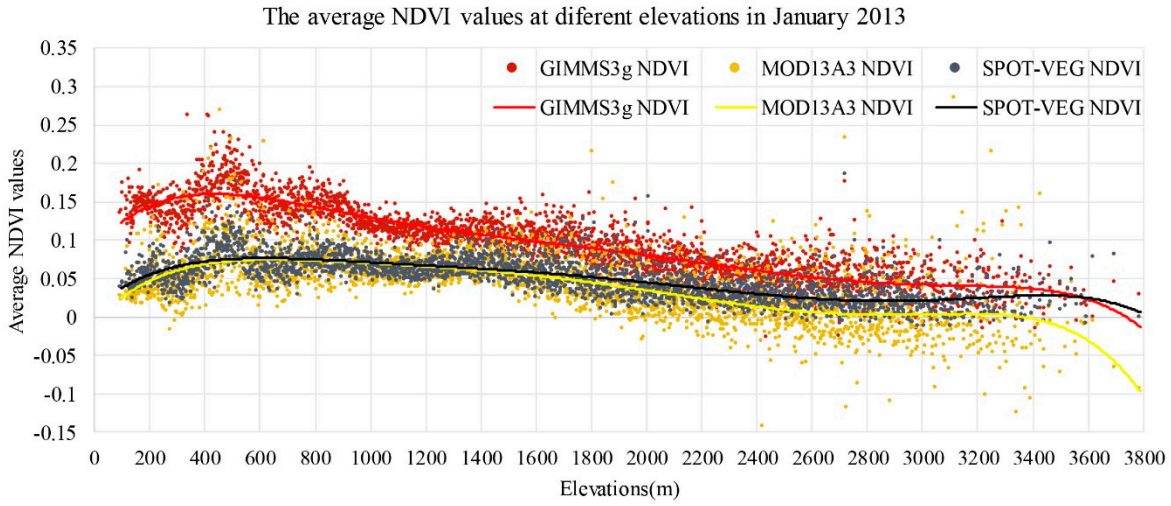


(**a**)

**Figure 10.** *Cont.*

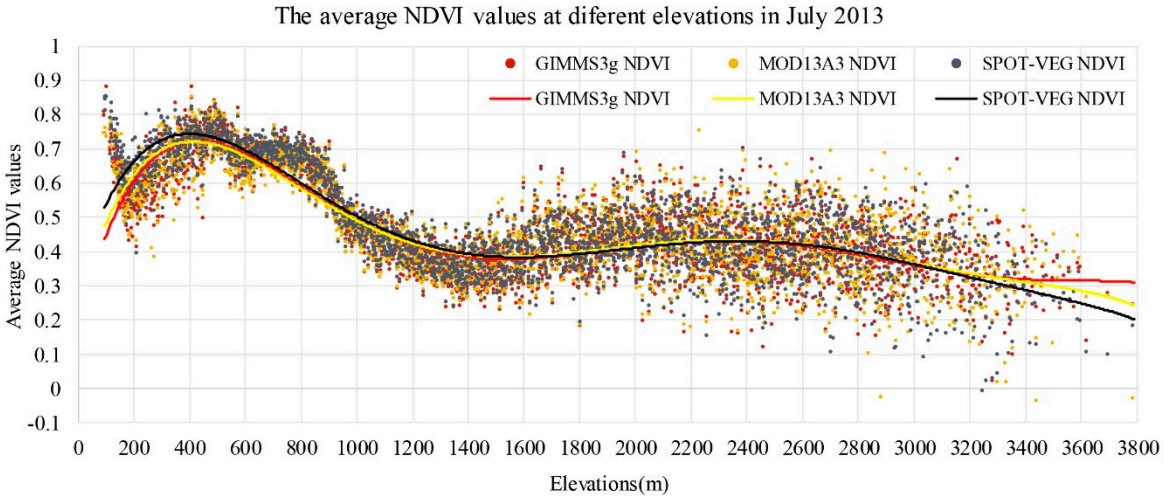


(**b**)

**Figure 10.** Scatter plots and fitting curves of average NDVI values at different elevations from 95 m to 3788 m in (**a**) January 2013 and (**b**) July 2013.

## 4. Discussion

### *4.1. Validation against Landsat-Based NDVI*

Based on the above results of the zonal differences of NDVI in the MP, 35 Landsat 8 images with very little cloud cover were selected to conduct the uniformity verification of the three NDVI datasets. Figure 11 presents the spatial distribution of the 35 Landsat 8 images in the MP, and the corresponding path/row and image date information for each Landsat 8 image are listed in Table 6. In order to analyze the consistency between Landsat 8-based NDVI and the other three NDVI datasets homogeneously, the 35 Landsat 8 images were resampled to the spatial resolution of GIMMS3g NDVI, MOD13A3 NDVI, and SPOT-VGT NDVI, respectively. Then, statistical scores were computed to describe the discrepancies between Landsat 8-based NDVI and the three NDVI products. Figure 12a shows the Pearson correlation coefficient between values of Landsat 8 NDVI and the corresponding three NDVI products. The mean values of the correlation coefficient between Landsat 8 NDVI and GIMMS3g NDVI, MOD13A3 NDVI, and SPOT-VGT NDVI are 0.57, 0.70, and 0.71, respectively. There are 19 Landsat 8 images with a Pearson correlation coefficient greater than 0.7 between MOD13A3 NDVI and SPOT-VGT NDVI values, and the higher coherence mostly occurred in late spring. As for GIMMS3g NDVI dataset, only seven Landsat 8 images have a Pearson correlation coefficient greater than 0.7 with corresponding GIMMS3g NDVI, and most of the low correlation coefficients are mainly distributed in winter and spring.

Figure 12b depicts the RMSE between Landsat 8 NDVI and the three NDVI datasets, in which the percentage of RMSE less than 0.1 between Landsat 8 NDVI and GIMMS3g NDVI, MOD13A3 NDVI, and SPOT-VGT NDVI are 54.71%, 68.57%, and 71.43%, respectively. Compared with the images in the eastern MP, the Landsat 8 images located in the northwest region of the MP are more different from the three NDVI datasets because of the higher RMSE values. The MBE between Landsat 8 NDVI values and the three datasets are depicted in Figure 12c. Same as the RMSE, the MBE values also have obvious longitude zonality, and the larger RMSE values generally correspond to larger MBE values. The values of Landsat 8 NDVI in the northeast of the MP are larger than the values of the other three NDVI datasets because of the positive MBE values. Conversely, the Landsat 8 NDVI values are essentially smaller than the three NDVI datasets in the northwest regions due to the negative MBE values. The proportion of Landsat 8 images with absolute values of MBE smaller than 0.05 between GIMMS3g NDVI, MOD13A3 NDVI, and SPOT-VGT NDVI are 77.14%, 74.29%, and 85.71%, respectively.

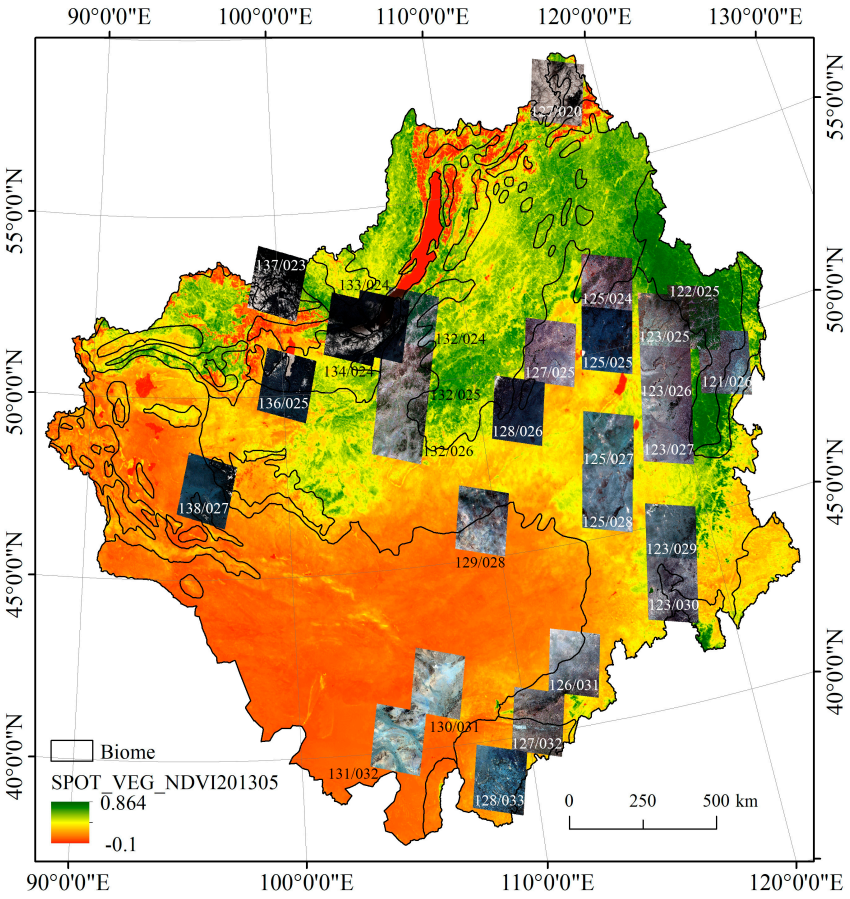


**Figure 11.** Spatial distribution of 35 Landsat 8 OLI/TIRS images for NDVI verification.

**Table 6.** Path/row and image date of 35 Landsat 8 images.

| Number | Path/Row | Image Date | Number | Path/Row | Image Date |
|---|---|---|---|---|---|
| 1 | 121/026 | 2014-04-15 | 19 | 128/033 | 2014-03-15 |
| 2 | 122/025 | 2014-05-24 | 20 | 128/033 | 2013-08-03 |
| 3 | 123/025 | 2014-04-29 | 21 | 128/033 | 2013-10-06 |
| 4 | 123/026 | 2014-04-29 | 22 | 128/033 | 2013-11-07 |
| 5 | 123/027 | 2014-04-29 | 23 | 128/033 | 2013-12-09 |
| 6 | 123/029 | 2014-04-29 | 24 | 129/028 | 2014-04-23 |
| 7 | 123/030 | 2014-04-29 | 25 | 130/031 | 2014-03-13 |
| 8 | 125/024 | 2014-04-27 | 26 | 131/032 | 2014-03-20 |
| 9 | 125/025 | 2014-04-27 | 27 | 132/024 | 2014-05-30 |
| 10 | 125/027 | 2014-05-29 | 28 | 132/025 | 2014-04-28 |
| 11 | 125/028 | 2014-04-27 | 29 | 132/025 | 2014-05-30 |
| 12 | 126/031 | 2014-05-20 | 30 | 132/026 | 2014-05-30 |
| 13 | 127/020 | 2014-04-09 | 31 | 133/024 | 2014-05-05 |
| 14 | 127/025 | 2013-10-15 | 32 | 134/024 | 2014-04-26 |
| 15 | 127/032 | 2013-08-12 | 33 | 136/025 | 2014-05-10 |
| 16 | 127/032 | 2013-09-29 | 34 | 137/023 | 2014-05-17 |
| 17 | 128/026 | 2014-03-31 | 35 | 138/027 | 2014-05-08 |
| 18 | 128/033 | 2014-01-26 | | | |

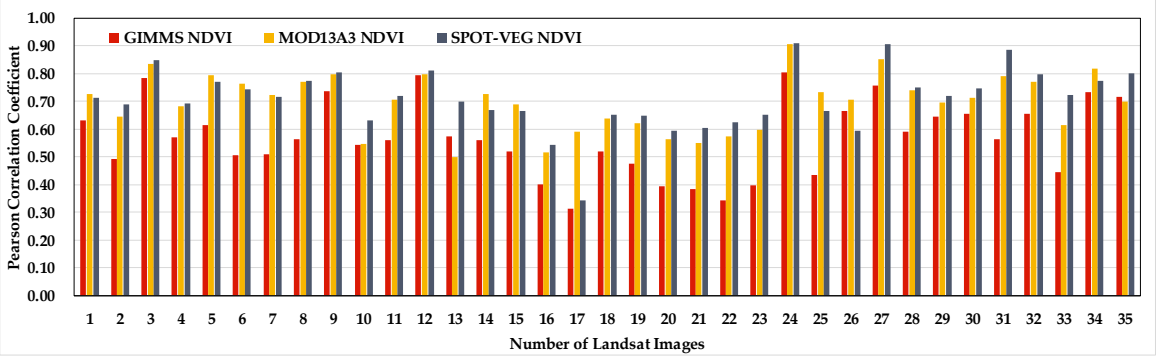


(**a**)

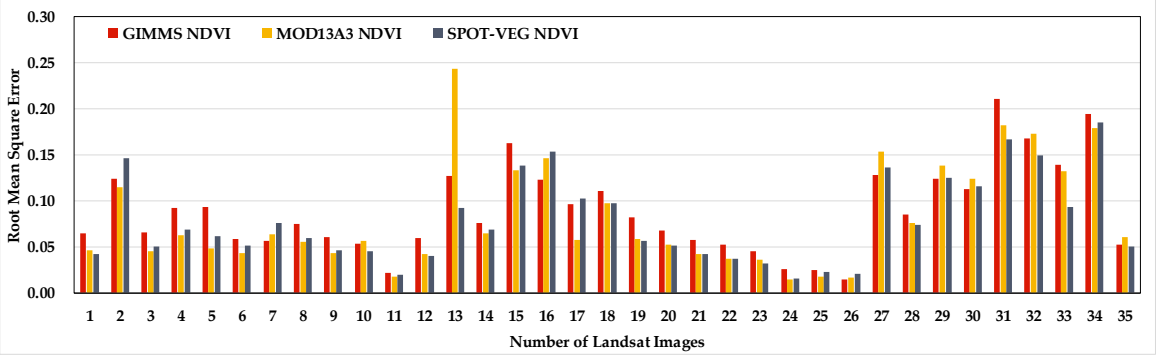


(**b**)

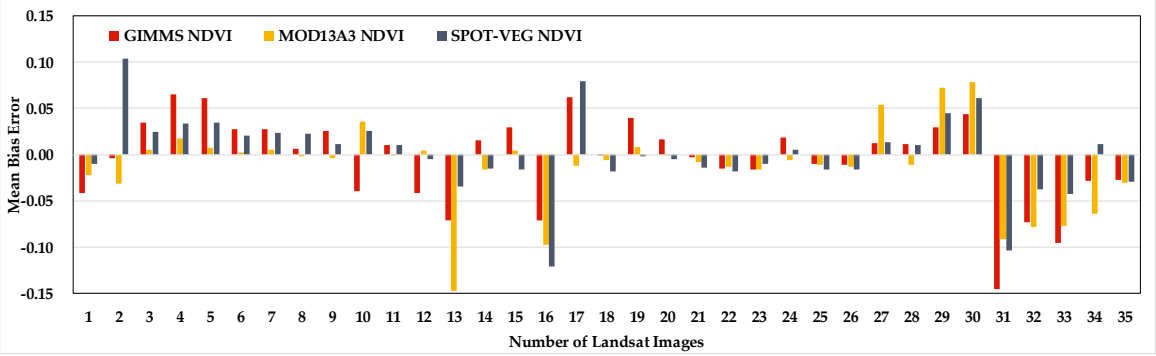


(**c**)

**Figure 12.** Consistency test results of Landsat 8 NDVI and the three NDVI products. (**a**) Pearson correlation coefficient; (**b**) root mean square error (RMSE); (**c**) mean bias error. The number of Landsat images in the figures corresponded to the number field in Table 6.

From the perspective of spatial distribution, the 35 Landsat images are scattered on different land cover types, such as forest, grassland, cropland, and bare/sandy land. Table 7 lists the mean values of statistic scores between Landsat 8-based NDVI and the corresponding three NDVI products over different land cover types in MP. There are seven Landsat 8 images (No. 1, 2, 8, 13, 31, 32, 34) that overlay the forest regions in the northern and eastern MP, in which the larger RMSE and smaller correlation coefficient between Landsat images and GIMMS3g NDVI indicate greater difference between these two datasets. On the contrary, SPOT-VGT NDVI has better consistency with Landsat 8-based NDVI in the forest regions in the MP. Grassland is one of the dominant land cover types in the MP, and there are 18 Landsat 8 images (No. 3–7, 10–12, 14–23) that overlay grassland, as shown in Figure 11. The NDVI values of grassland are greatly affected by seasonal changes, and the response

sensitivity of different satellite platforms to vegetation phenology is different, which leads to lower correlation between Landsat 8 images and the three NDVI products in grassland areas compared with other land cover types. In addition, some Landsat images may cover more than one type of land cover, which also can affect the consistency. SPOT-VGT NDVI has a larger correlation coefficient with Landsat 8 images, but the values of MOD13A3 NDVI are closer to Landsat 8-based NDVI.

**Table 7.** Average values of statistic scores between Landsat 8-based NDVI and the corresponding three NDVI products over different land cover types in the MP.

| Land Cover Types | Mean Correlation Coefficient | | | Mean RMSE | | | Mean MBE | | |
|---|---|---|---|---|---|---|---|---|---|
| | GIMMS3g | MOD13A3 | SPOT-VGT | GIMMS3g | MOD13A3 | SPOT-VGT | GIMMS3g | MOD13A3 | SPOT-VGT |
| Forest | 0.6056 | 0.7112 | 0.7226 | 0.2147 | 0.1503 | 0.1422 | −0.0561 | −0.0722 | −0.0758 |
| Grassland | 0.5009 | 0.6620 | 0.6674 | 0.0781 | 0.0613 | 0.0687 | −0.0070 | −0.0047 | −0.0272 |
| Cropland | 0.6342 | 0.7371 | 0.7696 | 0.1612 | 0.1128 | 0.1085 | −0.0106 | 0.0161 | −0.0511 |
| Bare/sandy land | 0.5975 | 0.7603 | 0.7068 | 0.0358 | 0.0275 | 0.0348 | −0.0137 | −0.0152 | −0.0254 |

Compared with other land cover types, the area of cropland in the MP is quite small. There are six Landsat 8 images (No. 9, 27–30, 33) that overlay cropland in the MP, based on Figures 2 and 11. The largest correlation coefficient and the lowest RMSE in the three combinations indicate that SPOT-VGT NDVI is the most consistent product with Landsat 8-based NDVI in cropland regions in the MP. Bare land and sandy land are the largest land cover types in the southwestern MP, and there are four Landsat 8 images (No. 24–26, 35) that overlay bare land and sandy land. Higher spectral resolution is more sensitive to identify NDVI in low vegetation coverage areas. Because the band ranges of Landsat 8 Operational Land Imager sensor are closer to Terra MODIS, Landsat 8-based NDVI values have higher correlation coefficient and lower RMSE with MOD13A3 NDVI values. Overall, SPOT-VGT NDVI is more consistent with Landsat 8-based NDVI in the land cover of forest, grassland, and cropland, while in bare land and sandy land, MOD13A3 NDVI products have better consistency with Landsat 8 NDVI.

Considering that the resampling process has certain influence on the accuracy of original datasets, four Landsat images with distinct time and location were selected to carry out visual comparison with the other three NDVI datasets (Figure 13). The first Landsat 8 image (path = 123, row = 027, image date: 2014-04-29) and the second image (path = 125, row = 027, image date: 2014-05-29) were selected because GIMMS3g NDVI, MOD13A3 NDVI, and SPOT-VGT NDVI demonstrated large discrepancy in spring in the eastern part of Mongolia. The third Landsat 8 image (path = 127, row = 032, image date: 2013-08-12) and the fourth image (path = 128, row = 033, image date: 2013-11-07) represented summer and autumn in the southern IMAR, respectively. It was found that the four NDVI datasets are similar in expressing surface vegetation, but there are inevitably some small-scale differences because of different spatial and temporal resolution. Among them, the Landsat 8 NDVI values are best matched with MOD13A3 NDVI values in spatial distribution.

The first column in Figure 13 reveals that MOD13A3 NDVI, SPOT-VGT NDVI, and Landsat 8 NDVI could identify more vegetation cover than GIMMS3g NDVI, and the spatial distribution of Landsat 8 NDVI values are much closer to the MOD13A3 NDVI. For the second column in Figure 13, the spatial distribution of MOD13A3 NDVI and SPOT-VGT NDVI are much more similar to Landsat 8 NDVI in expressing the surface vegetation than GIMMS3g NDVI, and GIMMS3g NDVI failed to describe the features in small areas. The third column in Figure 13 explains the best coherence of the four NDVI datasets with vegetation identified well in summer, and all four datasets could better distinguish the vegetation from background, in which MOD13A3 NDVI, SPOT-VGT NDVI, and Landsat 8 NDVI could identify more detailed surface information because of their higher spatial resolution. The last column in Figure 13 reveals that GIMMS3g NDVI has weaker recognition of vegetation in later autumn, and its coarse resolution resulted in many loses of specific information. On the contrary, the spatial distributions of NDVI of other three datasets with higher resolution were relatively consistent.

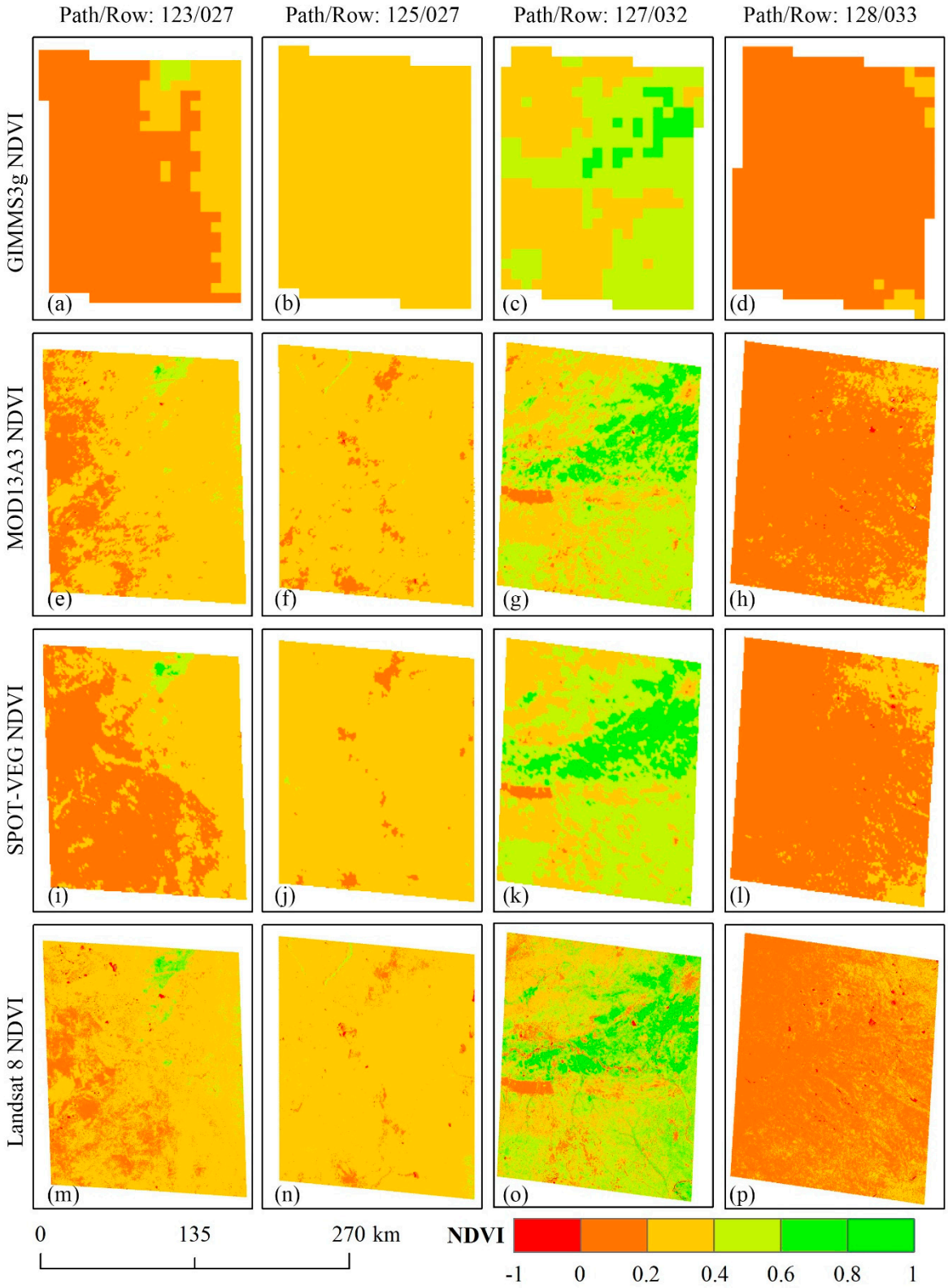


**Figure 13.** Contrastive analysis of GIMMS3g NDVI (**a**–**d**), MOD13A3 NDVI (**e**–**h**), SPOT-VGT NDVI (**i**–**l**) and Landsat 8 NDVI (**m**–**p**) in different time and space ranges. The Path/Row in the figure represents the path and row number of Landsat 8 images.

In general, Landsat 8 data could effectively recognize the fine features of surface vegetation because of its high spatial resolution. It was revealed that MOD13A3 NDVI and SPOT-VGT NDVI

values have higher spatial distribution consistency with Landsat 8 NDVI values and best matching results through visual comparison analysis, while GIMMS NDVI often neglects the small surface features because of its coarse resolution, resulting in less accurate vegetation expression than other NDVI datasets. By resampling to the same resolution, the statistic scores between Landsat 8 NDVI and three NDVI datasets indicate that SPOT-VGT NDVI have higher consistencies with Landsat 8 NDVI than GIMMS3g NDVI and MOD13A3 NDVI. In addition, the agreements between different NDVI datasets vary longitudinally and zonally, and the consistencies in the northeast of the MP are higher than northwest regions.

### *4.2. Influencing Factors of NDVI Consistency*

The intercomparison study of three satellite NDVI products in the MP revealed some discrepancy. The results show that the distribution and the scope of biomes, basically corresponding to various land cover types, have obvious influence on the spatial variance of NDVI values. Vegetated areas have better NDVI agreement than non-vegetated surfaces. Changes of climate and meteorological factors determine the phenology of vegetation, which affects the exchange of crop-atmospheric energy, water, and carbon [70,71], thus the differences between the three datasets fluctuate with the change of latitudes, longitudes, and elevation. Consequently, the three NDVI datasets of the MP have obvious seasonal variation characteristics and regional differentiation rules. According to the intercomparison results, there are some inconsistencies among the three datasets during the succession of the MP. The major reasons that make the three NDVI datasets vary differently can be summed up as follows:

First of all, the three datasets are produced from different satellite with different sensor designs. The differences in spectral band responses, instrument performances, and atmospheric conditions at the time of observation increase inconsistencies in measuring surface reflectance [72]. Teillet and Ren [73] pointed out that the differences in spectral wavelength of various sensors alone can lead to as large as 10% of the NDVI differences. Compared with AVHRR and VEGETATION, the MODIS sensor has higher radiometric and spatial resolution and narrower spectral range of red and near-infrared (NIR) band. The red bands govern chlorophyll sensitivity, and thereby influence the annual NDVI range [74]. The narrower NIR bands are more sensitive to atmospheric conditions [72], which can identify vegetation characteristics and capture details of vegetation changes more accurately. Different from the narrower NIR bands of MODIS and VEGETATION sensor, the AVHRR NIR band is superimposed on strong water vapor absorption bands between 900–980 nm [74]. Also the discontinuity of sensor shifts may affect the trend analysis in semi-arid regions, such as the sensor shifts from NOAA-16, NOAA-17, to NOAA-18 for GIMMS3g NDVI and from SPOT-4 to SPOT-5 for SPOT-VGT NDVI datasets [74,75]. It has been proved in the related research of vegetation phenology recognition that spatial resolution has little influence on trend analysis of time series variation [74,76]. In this work, the three NDVI products were compared and contrasted in different spatial resolution, and Figure 14 shows the trend components of decomposed average values of the three datasets in the spatial resolution of GIMMS3g NDVI (about 8 km) and MOD13A3 NDVI (about 1 km), respectively. The change trends of each data set are almost the same at two different spatial resolutions, which indicates that the influence of spatial resolution of satellite sensor on NDVI variation trends can be neglected in the MP.

Secondly, the three satellites have different platform characteristics and sensor viewing conditions. The visit frequency of the satellite determines the temporal resolution of datasets. The NOAA series have the highest visit frequency because of the large number of satellites, while the SPOT satellite has the longest return interval. The overpass time of satellites is an essential basis of the image quality. Meanwhile, different atmospheric conditions could lead to considerable difference in surface NDVI. The weather conditions, such as atmospheric visibility, cloud shadows, cirrus, and aerosol amounts, are also key factors for image quality. Large scale events like El Niño/La Niña and volcanic eruption may also cause vegetation changes on global or regional scales [76,77]. It was found that solar zenith angles have small influence in NDVI simulations, but it should be noted that bidirectional reflectance

distribution function (BRDF) differences between the two sensors caused by different azimuth angles and rugged terrains could be considerable [72].

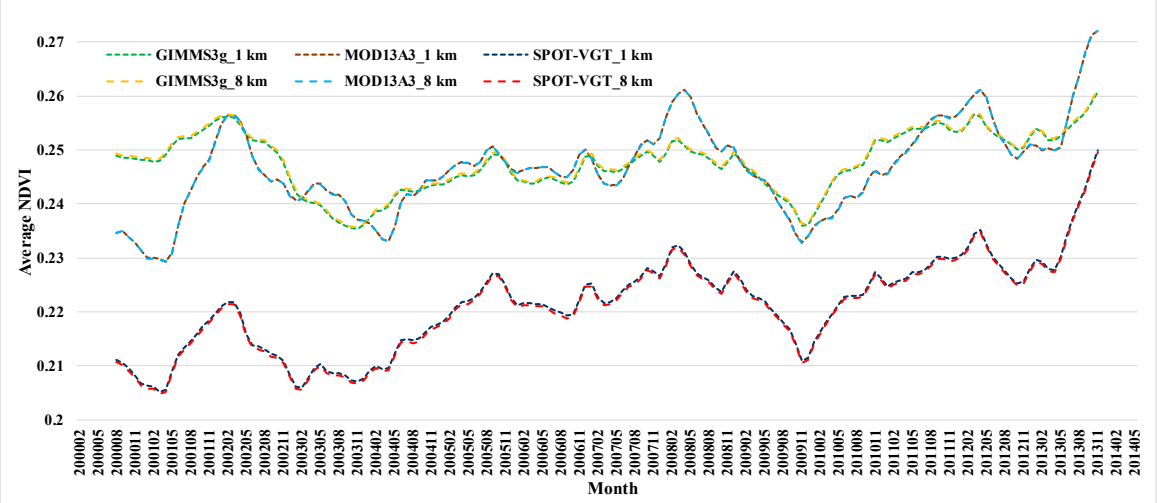


**Figure 14.** Trend components of decomposed average values of GIMMS3g NDVI, MOD13A3 NDVI, and SPOT-VGT NDVI in different spatial resolution (1 km and 8 km) in the MP.

At last, the data processing techniques affect the NDVI variation noticeably. Usually, the images acquired by satellites are deformed to some extent, which requires strict atmospheric and geometric correction before calculation and scientific practice. On the other hand, the processing methods used in practical applications are also coordinated aspects leading to data differences. According to the dataset documents, monthly MOD13A3 NDVIs are composited by weighted temporal average of all the 16-day MOD13A2 products that overlap the month. In order to reduce the difference between diverse datasets, the average synthesis method is also used in processing of GIMMS3g NDVI and SPOT-VGT NDVI. Correspondingly, GIMMS3g NDVI and SPOT-VGT NDVI datasets are also resampled to monthly values by the means of averaging calculation. It is predicted that the cloud contamination and the actual changes at small scale are balanced out when averaging the NDVI values on regional scale, but the drawback of the synthesis methodology is the loss of critical temporal information required to accurately track the processes of vegetation change [71,74,76]. From a spatial point of view, the MOD13A3 NDVI and SPOT-VGT NDVI datasets were resampled to the spatial resolution of GIMMS3g NDVI by bilinear interpolation method in order to facilitate the intercomparison. For higher resolution data such as MOD13A3 NDVI and SPOT-VGT NDVI, this upscale method generalizes the information of small surface features to some extent, but it still can effectively reveal the consistency of trend analysis of long time series data.

Therefore, our results may contain uncertainties introduced by the differences of parameters between satellite platform and sensor system. Even though some systematic errors can be reduced by geometric correction and atmospheric correction, it is impossible to eliminate all errors completely. Because of the inconsistent spatial and temporal resolution of various datasets, the processing methods used in this work, including spatial resample, temporal composite, average extraction, and so on, also increase the errors among three datasets in varying degree. The reasons behind these discrepancies need to be further explored, since a growing volume of studies within vegetation and climate change research is based on these long-term datasets.

## 5. Conclusions

This study aimed for intercomparison of three global NDVI products, namely, GIMMS3g NDVI, MOD13A3 NDVI, and SPOT-VGT NDVI over the MP from February 2000 to May 2014. Averaged NDVI values are in decreasing order of GIMMS3g NDVI, MOD13A3 NDVI, and SPOT-VGT NDVI, based on

the comparative analysis of temporal evolution, spatial distribution, and regional differentiation of the three NDVI products. The decomposed NDVI sequences show that the three NDVI datasets have similar variation trends, but SPOT-VGT NDVI values are about 0.02 lower than the other two datasets in the whole variation periods. The spatial distributions of the AC values indicate that the three NDVI datasets are highly consistent with each other in the northern regions of the MP, and MOD13A3 NDVI and SPOT-VGT NDVI have better consistency in expressing vegetation cover and change trends in the MP from February 2000 to May 2014. The MBE values show that SPOT-VGT NDVI values are significantly smaller than the values of GIMMS3g NDVI and MOD13A3 NDVI, while GIMMS3g NDVI values are relatively larger than MOD13A3 NDVI values in the northern MP, but contrary to those in the southern MP.

NDVI changes in the seven biomes are full of discrepancy due to the diversity of surface land cover. The SPOT-VGT NDVI values are generally lower than the other two datasets, and the difference expands with the increase of surface vegetation coverage. Deseasonalized values of MOD13A3 NDVI show higher discreteness than the other two datasets by STD over various biomes and the whole of the MP. Taking 2013 as an example, the zonal characteristics of latitude, longitude, and elevation show that GIMMS3g NDVI in January 2013 are significantly higher than those of the other two datasets. However, in July 2013, the three datasets are remarkably consistent. The results of vertical zonal statistical analysis show that NDVI values decrease with the increase of altitude.

Consistency validation results of three NDVI products against Landsat 8 images show that values of SPOT-VGT NDVI agree more with Landsat 8 NDVI than GIMMS3g NDVI and MOD13A3 NDVI, and the consistencies in the northeast of the MP are higher than northwest regions. The other two NDVI datasets, especially GIMMS3g NDVI, are higher than Landsat 8-based NDVI values in varying degrees. Hence, we believe that our study helps to deepen understanding of largescale vegetation variation trends over the MP, which would significantly enhance our knowledge of the potential future impact of climate warming on inland areas of the Northern Hemisphere and provide important reference for the follow-up study on vegetation change in Northern Asia.

**Author Contributions:** All authors assisted in data analysis and manuscript preparation of the paper. Y.B. and Y.Y. conceived and designed the experiments; H.J. and Y.B. performed the experiments and analyzed the data; Y.Y. contributed analysis tools; and Y.B. wrote the paper.

**Funding:** This research was funded by the Special Project of Scientific and Technological Fundamental Resources Survey in China (2017FY101300), National Earth System Science Data Center (http://www.geodata.cn/) (2005DKA32300), China Knowledge Center for Engineering Sciences and Technology-Geography Resources and Ecology Knowledge Service System (http://geo.ckcest.cn/) (CKCEST-2019-1-4).

**Conflicts of Interest:** The authors declare no conflicts of interest.

## References

1. Cao, M.; Woodward, F.I. Dynamic responses of terrestrial ecosystem carbon cycling to global climate change. *Nature* **1998**, *393*, 249–252. [CrossRef]
2. Fan, L.; Gao, Y.; Brück, H.; Bernhofer, C. Investigating the relationship between NDVI and LAI in semi-arid grassland in Inner Mongolia using in-situ measurements. *Theor. Appl. Climatol.* **2009**, *95*, 151–156. [CrossRef]
3. Yuhas, A.N.; Scuderi, L.A. MODIS—Derived NDVI characterisation of drought—Induced evergreen dieoff in Western North America. *Geogr. Res.* **2010**, *47*, 34–45. [CrossRef]
4. Li, M.; Wu, B.; Yan, C.; Zhou, W. Estimation of vegetation fraction in the upper basin of Miyun Reservoir by remote sensing. *Resour. Sci.* **2004**, *26*, 153–159.
5. Bannari, A.; Morin, D.; Bonn, F.; Huete, A.R. A review of vegetation indices. *Remote Sens. Rev.* **1995**, *13*, 95–120. [CrossRef]
6. Guo, N. Vegetation Index and Its Advances. *J. Arid Meteorol.* **2003**, *21*, 71–75.
7. Guo, N.; Yang, L.; Wang, J. A Study of Ecological Environment in Heihe Valley Area through Meteorology Satellite Monitoring. *Plateau Meteorol.* **2002**, *21*, 267–273.
8. Roerink, G.J.; Menenti, M.; Soepboer, W.; Su, Z. Assessment of climate impact on vegetation dynamics by using remote sensing. *Phys. Chem. Earth* **2002**, *28*, 103–109. [CrossRef]

9. Landmann, T.; Schramm, M.; Huettich, C.; Dech, S. MODIS-based change vector analysis for assessing wetland dynamics in Southern Africa. *Remote Sens. Lett.* **2013**, *4*, 104–113. [CrossRef]
10. Price, J.C. Using spatial context in satellite data to infer regional scale evapotranspiration. *IEEE Trans. Geosci. Remote Sens.* **1990**, *28*, 940–948. [CrossRef]
11. Carlson, T.N.; Gillies, R.R.; Perry, E.M. A Method to Make Use of Thermal Infrared Temperature and NDVI measurements to Infer Surface Soil Water Content and Fractional Vegetation Cover. *Remote Sens. Rev.* **1994**, *9*, 161–173. [CrossRef]
12. Anyamba, A.; Tucker, C.J. Analysis of Sahelian vegetation dynamics using NOAA-AVHRR NDVI data from 1981–2003. *J. Arid Environ.* **2005**, *63*, 596–614. [CrossRef]
13. Moulin, S.; Kergoat, L.; Viovy, N.; Dedieu, G. Global-Scale Assessment of Vegetation Phenology Using NOAA/AVHRR Satellite Measurements. *J. Clim.* **1995**, *10*, 1154–1170. [CrossRef]
14. Xin, J.; Yu, Z.; Leeuwen, L.V.; Driessen, P.M. Mapping crop key phenological stages in the North China Plain using NOAA time series images. *Int. J. Appl. Earth Obs. Geoinf.* **2003**, *4*, 109–117. [CrossRef]
15. Hermance, J.F.; Jacob, R.W.; Bradley, B.A.; Mustard, J.F. Extracting Phenological Signals from Multiyear AVHRR NDVI Time Series: Framework for Applying High-Order Annual Splines with Roughness Damping. *IEEE Trans. Geosci. Remote Sens.* **2007**, *45*, 3264–3276. [CrossRef]
16. Duarte, L.; Teodoro, A.C.; Monteiro, A.T.; Cunha, M.; Gonçalves, H. QPhenoMetrics: An open source software application to assess vegetation phenology metrics. *Comput. Electron. Agric.* **2018**, *148*, 82–94. [CrossRef]
17. Chen, X.; Tan, Z.; Schwartz, M.D.; Xu, C. Determining the growing season of land vegetation on the basis of plant phenology and satellite data in Northern China. *Int. J. Biometeorol.* **2000**, *44*, 97–101. [CrossRef]
18. Bradley, B.A.; Jacob, R.W.; Hermance, J.F.; Mustard, J.F. A curve fitting procedure to derive inter-annual phenologies from time series of noisy satellite NDVI data. *Remote Sens. Environ.* **2007**, *106*, 137–145. [CrossRef]
19. Zhang, G.; Zhang, Y.; Dong, J.; Xiao, X. Green-up dates in the Tibetan Plateau have continuously advanced from 1982 to 2011. *Proc. Natl. Acad. Sci. USA* **2013**, *110*, 4309–4314. [CrossRef]
20. Jeong, S.J.; Ho, C.H.; Brown, M.E.; Kug, J.S.; Piao, S. Browning in desert boundaries in Asia in recent decades. *J. Geophys. Res. Atmos.* **2011**, *116*, 1–7. [CrossRef]
21. Waweru, M.N.; Jahjah, M.; Laneve, G. Spatial change analysis using temporal remote sensing and ancillary data for desertification change detection. *Proc. SPIE Int. Soc. Opt. Eng.* **2004**, *5239*, 345–356.
22. Saito, H.; Sawada, Y.; Furuya, N.; Preap, S. *Land Cover Change Mapping of the Mekong River Basin Using NOAA Pathfinder AVHRR 8-km Land Dataset*; Springer: New York, NY, USA, 2007.
23. Brown, J.C.; Kastens, J.H.; Coutinho, A.C.; de Castro Victoria, D.; Bishop, C.R. Classifying multiyear agricultural land use data from Mato Grosso using time-series MODIS vegetation index data. *Remote Sens. Environ.* **2013**, *130*, 39–50. [CrossRef]
24. Gopal, S.; Woodcock, C.E.; Strahler, A.H. Fuzzy Neural Network Classification of Global Land Cover from a 1° AVHRR Data Set. *Remote Sens. Environ.* **1999**, *67*, 230–243. [CrossRef]
25. Hill, M.J.; Vickery, P.J.; Furnival, E.P.; Donald, G.E. Pasture Land Cover in Eastern Australia from NOAA-AVHRR NDVI and Classified Landsat TM. *Remote Sens. Environ.* **1999**, *67*, 32–50. [CrossRef]
26. Pan, Y.; Li, X.; Gong, P.; He, C.; Shi, P.; Pu, R. An integrative classification of vegetation in China based on NOAA AVHRR and vegetation-climate indices of the Holdridge life zone. *Int. J. Remote Sens.* **2003**, *24*, 1009–1027. [CrossRef]
27. Bisson, M.; Fornaciai, A.; Coli, A.; Mazzarini, F.; Pareschi, M.T. The Vegetation Resilience after Fire (VRAF) index: Development, implementation and an illustration from central Italy. *Int. J. Appl. Earth Obs. Geoinf.* **2008**, *10*, 312–329. [CrossRef]
28. Chuvieco, E.; Martín, M.P.; Palacios, A. Assessment of different spectral indices in the red-near-infrared spectral domain for burned land discrimination. *Int. J. Remote Sens.* **2002**, *23*, 5103–5110. [CrossRef]
29. Escuin, S.; Navarro, R.; Fernández, P. Fire severity assessment by using NBR (Normalized Burn Ratio) and NDVI (Normalized Difference Vegetation Index) derived from LANDSAT TM/ETM images. *Int. J. Remote Sens.* **2008**, *29*, 21. [CrossRef]
30. John, R.; Chen, J.; Ouyang, Z.T.; Xiao, J.; Becker, R.; Samanta, A.; Ganguly, S.; Yuan, W.; Batkhishig, O. Vegetation response to extreme climate events on the Mongolian Plateau from 2000 to 2010. *Environ. Res. Lett.* **2013**, *8*, 035033. [CrossRef]

31. Bunkei, M.; Wei, Y.; Jin, C.; Yuyichi, O.; Guoyu, Q. Sensitivity of the Enhanced Vegetation Index (EVI) and Normalized Difference Vegetation Index (NDVI) to Topographic Effects: A Case Study in High-density Cypress Forest. *Sensors* **2007**, *7*, 2636–2651.
32. Jiang, Z.; Huete, A.R.; Didan, K.; Miura, T. Development of a two-band enhanced vegetation index without a blue band. *Remote Sens. Environ.* **2008**, *112*, 3833–3845. [CrossRef]
33. Chu, H.; Venevsky, S.; Wu, C.; Wang, M. NDVI-based vegetation dynamics and its response to climate changes at Amur-Heilongjiang River Basin from 1982 to 2015. *Sci. Total Environ.* **2019**, *650*, 2051–2062. [CrossRef] [PubMed]
34. Zheng, K.; Wei, J.; Pei, J.; Cheng, H.; Zhang, X.; Huang, F.; Li, F.; Ye, J. Impacts of climate change and human activities on grassland vegetation variation in the Chinese Loess Plateau. *Sci. Total Environ.* **2019**, *660*, 236–244. [CrossRef] [PubMed]
35. Gu, Y.; Wylie, B.K.; Howard, D.M.; Phuyal, K.P.; Lei, J.I. NDVI saturation adjustment: A new approach for improving cropland performance estimates in the Greater Platte River Basin, USA. *Ecol. Indic.* **2013**, *30*, 1–6. [CrossRef]
36. Du, J.Q.; Shu, J.M.; Wang, Y.H.; Li, Y.C.; Yang, G. Comparison of GIMMS and MODIS normalized vegetation index composite data for Qinghai-Tibet Plateau. *Chin. J. Appl. Ecol.* **2014**, *25*, 533.
37. Fensholt, R.; Proud, S.R. Evaluation of Earth Observation based global long term vegetation trends-Comparing GIMMS and MODIS global NDVI time series. *Remote Sens. Environ.* **2012**, *119*, 131–147. [CrossRef]
38. Hou, M.; Zhao, H.; Wang, Z.; Yan, X. Comparison of GIMMS, VGT and MODIS Vegetation Index Datasets in Eastern China. *Remote Sens. Technol. Appl.* **2013**, *28*, 290–299.
39. Zhou, X.; Yamaguchi, Y.; Arjasakusuma, S. Distinguishing the vegetation dynamics induced by anthropogenic factors using vegetation optical depth and AVHRR NDVI: A cross-border study on the Mongolian Plateau. *Sci. Total Environ.* **2018**, *616–617*, 730–743. [CrossRef]
40. Suzuki, R.; Masuda, K.; Dye, D.G. Interannual covariability between actual evapotranspiration and PAL and GIMMS NDVIs of northern Asia. *Remote Sens. Environ.* **2007**, *106*, 387–398. [CrossRef]
41. Ibrahim, Y.Z.; Balzter, H.; Kaduk, J.; Tucker, C.J. Land Degradation Assessment Using Residual Trend Analysis of GIMMS NDVI3g, Soil Moisture and Rainfall in Sub-Saharan West Africa from 1982 to 2012. *Remote Sens.* **2015**, *7*, 5471–5494. [CrossRef]
42. Meng, D.; Xiaojuan, L.I.; Gong, H.; Yiting, Q.U. Analysis of Spatial-Temporal Change of NDVI and Its Climatic Driving Factors in Beijing-Tianjin-Hebei Metropolis Circle from 2001 to 2013. *J. Geo-Inf. Sci.* **2015**, *17*, 1001–1007.
43. Bilal, M.; Nichol, J.E. Evaluation of the NDVI-Based Pixel Selection Criteria of the MODIS C6 Dark Target and Deep Blue Combined Aerosol Product. *IEEE J. Sel. Top. Appl. Earth Obs. Remote Sens.* **2017**, *10*, 3448–3453. [CrossRef]
44. Miao, L.; Jiang, C.; Xue, B.; Liu, Q.; He, B.; Nath, R.; Cui, X. Vegetation dynamics and factor analysis in arid and semi-arid Inner Mongolia. *Environ. Earth Sci.* **2015**, *73*, 2343–2352. [CrossRef]
45. Chang, N.-B. Using SPOT-VGT NDVI as a successive ecological indicator for understanding the environmental implications in the Tarim River Basin, China. *J. Appl. Remote Sens.* **2010**, *4*, 844–862. [CrossRef]
46. Hou, X.; Gao, S.; Niu, Z.; Xu, Z. Extracting grassland vegetation phenology in North China based on cumulative SPOT-VEGETATION NDVI data. *Int. J. Remote Sens.* **2014**, *35*, 3316–3330. [CrossRef]
47. Beck, H.E.; McVicar, T.R.; van Dijk, A.I.; Schellekens, J.; de Jeu, R.A.; Bruijnzeel, L.A. Global evaluation of four AVHRR-NDVI data sets: Intercomparison and assessment against Landsat imagery. *Remote Sens. Environ.* **2011**, *115*, 2547–2563. [CrossRef]
48. Gallo, K.; Lei, J.; Reed, B.; Eidenshink, J.; Dwyer, J. Multi-platform comparisons of MODIS and AVHRR normalized difference vegetation index data. *Remote Sens. Environ.* **2005**, *99*, 221–231. [CrossRef]
49. Fensholt, R.; Rasmussen, K.; Nielsen, T.T.; Mbow, C. Evaluation of earth observation based long term vegetation trends—Intercomparing NDVI time series trend analysis consistency of Sahel from AVHRR GIMMS, Terra MODIS and SPOT VGT data. *Remote Sens. Environ.* **2009**, *113*, 1886–1898. [CrossRef]
50. Song, F.; Kang, M.; Yang, P.; Chen, Y.; Liu, Y.; Xing, K. Comparison and validation of GIMMS, SPOT-VGT and MODIS global NDVI products in the Loess Plateau of northern Shaanxi Province, northwestern China. *J. Beijing For. Univ.* **2010**, *32*, 78–86.

51. Bao, G.; Bao, Y.; Qin, Z.; Zhou, Y.; Adiya, S. Vegetation Cover Changes in Mongolian Plateau and Its Response to Seasonal Climate Changes in Recent 10 Years. *Sci. Geogr. Sin.* **2013**, *33*, 613–621.
52. Wang, L.; Zhen, L.; Liu, X.; Batkhishig, O.; Wang, Q. Comparative studies on climate changes and influencing factors in central Mongolian Plateau Region. *Geogr. Res.* **2008**, *27*, 171–180.
53. Zhou, X.; Shi, H.; Wang, X.; Meng, F. Study on the temporal and spatial dynamic changes of land use and driving forces analysis of Mongolia Plateau in recent 30 years. *Acta Agric. Zhejiangensis* **2012**, *24*, 0–1110.
54. Du, J.; Kimball, J.S.; Galantowicz, J.; Kim, S.B.; Chan, S.K.; Reichle, R.; Jones, L.A.; Watts, J.D. Assessing global surface water inundation dynamics using combined satellite information from SMAP, AMSR2 and Landsat. *Remote Sens. Environ.* **2018**, *213*, 1–17. [CrossRef] [PubMed]
55. GLOBCOVER 2009: Products Description and Validation Report. Available online: http://due.esrin.esa.int/files/GLOBCOVER2009_Validation_Report_2.2.pdf (accessed on 28 August 2019).
56. Niu, Z.; Shan, Y.; Zhang, H. Accuracy assessment of wetland categories from the GlobCover2009 data over China. *Wetl. Sci.* **2012**, *10*, 389–395.
57. Olson, D.M.; Dinerstein, E.; Wikramanayake, E.D.; Burgess, N.D.; Powell, G.V.N.; Underwood, E.C.; D'Amico, J.A.; Itoua, I.; Strand, H.E.; Morrison, J.C. Terrestrial Ecoregions of the World: A New Map of Life on Earth. *Bioscience* **2001**, *51*, 933–938. [CrossRef]
58. Roy, D.P.; Wulder, M.A.; Loveland, T.R.; Woodcock, C.E.; Allen, R.G.; Anderson, M.C.; Helder, D.; Irons, J.R.; Johnson, D.M.; Kennedy, R. Landsat-8: Science and product vision for terrestrial global change research. *Remote Sens. Environ.* **2014**, *145*, 154–172. [CrossRef]
59. Rouse, J.W.; Haas, R.H.; Schell, J.A.; Deering, D.W. Monitoring Vegetation Systems in the Great Plains with ERTS. In *Third Earth Resources Technology Satellite-1 Symposium*; Freden, S.C., Mercanti, E.P., Becker, M.A., Eds.; University of California Libraries: Berkeley, CA, USA, 1974.
60. Ji, L.; Gallo, K. An Agreement Coefficient for Image Comparison. *Photogramm. Eng. Remote Sens.* **2015**, *73*, 823–833. [CrossRef]
61. Jing, W.; Zhang, P.; Zhao, X. A comparison of different GRACE solutions in terrestrial water storage trend estimation over Tibetan Plateau. *Sci. Rep.* **2019**, *9*, 1765. [CrossRef]
62. Andrew, R.; Guan, H.; Batelaan, O. Estimation of GRACE Water Storage Components by Temporal Decomposition. *J. Hydrol.* **2017**, *552*, 341–350. [CrossRef]
63. Verbesselt, J.; Zeileis, A.; Herold, M. Near real-time disturbance detection using satellite image time series. *Remote Sens. Environ.* **2012**, *123*, 98–108. [CrossRef]
64. Bai, Y.; Wang, J.; Wang, Y.; Han, X.; Tsydypov, B.Z.; Ochir, A.; Davaasuren, D. Spatio-Temporal Distribution of Drought in the Belt and Road Area During 1998–2015 Based on TRMM Precipitation Data. *J. Resour. Ecol.* **2017**, *8*, 559–570.
65. Lu, H.; Raupach, M.R.; Mcvicar, T.R.; Barrett, D.J. Decomposition of vegetation cover into woody and herbaceous components using AVHRR NDVI time series. *Remote Sens. Environ.* **2003**, *86*, 1–18. [CrossRef]
66. Kendall, M.G. *The Advanced Theory of Statistics*; Charles Griffin and Co., Ltd.: London, UK, 1946.
67. Bao, G.; Qin, Z.H.; Bao, Y.H.; Zhou, Y. Spatial-temporal Changes of Vegetation Cover in Mongolian Plateau during 1982—2006. *J. Desert Res.* **2013**, *33*, 918–927.
68. Dymond, C.C.; Johnson, E.A. Mapping vegetation spatial patterns from modeled water, temperature and solar radiation gradients. *ISPRS J. Photogramm. Remote Sens.* **2002**, *57*, 69–85. [CrossRef]
69. Hu, S.; Zhao, R.; Jia, Y.; Niu, C.; Liu, L.; Zhan, C. The characteristic of vegetation vertical zonality and the influential factors in typical mountains in China. *Chin. J. Nat.* **2018**, *40*, 12–16.
70. Ahl, D.E.; Gower, S.T.; Burrows, S.N.; Shabanov, N.V.; Myneni, R.B.; Knyazikhin, Y. Monitoring spring canopy phenology of a deciduous broadleaf forest using MODIS. *Remote Sens. Environ.* **2006**, *104*, 88–95. [CrossRef]
71. Liu, Z.; Wu, C.; Liu, Y.; Wang, X.; Fang, B.; Yuan, W.; Ge, Q. Spring green-up date derived from GIMMS3g and SPOT-VGT NDVI of winter wheat cropland in the North China Plain. *ISPRS J. Photogramm. Remote Sens.* **2017**, *130*, 81–91. [CrossRef]
72. Ke, Y.; Im, J.; Lee, J.; Gong, H.; Ryu, Y. Characteristics of Landsat 8 OLI-derived NDVI by comparison with multiple satellite sensors and in-situ observations. *Remote Sens. Environ.* **2015**, *164*, 298–313. [CrossRef]
73. Teillet, P.M.; Ren, X. Spectral band difference effects on vegetation indices derived from multiple satellite sensor data. *Can. J. Remote Sens.* **2008**, *34*, 159–173.

74. Fontana, F.; Rixen, C.; Jonas, T.; Aberegg, G.; Wunderle, S. Alpine Grassland Phenology as Seen in AVHRR, VEGETATION, and MODIS NDVI Time Series—A Comparison with in Situ Measurements. *Sensors* **2008**, *8*, 2833–2853. [CrossRef]
75. Tian, F.; Fensholt, R.; Verbesselt, J.; Grogan, K.; Horion, S.; Wang, Y. Evaluating temporal consistency of long-term global NDVI datasets for trend analysis. *Remote Sens. Environ.* **2015**, *163*, 326–340. [CrossRef]
76. Kross, A.; Fernandes, R.; Seaquist, J.; Beaubien, E. The effect of the temporal resolution of NDVI data on season onset dates and trends across Canadian broadleaf forests. *Remote Sens. Environ.* **2011**, *115*, 1564–1575. [CrossRef]
77. Lucht, W.; Prentice, I.C.; Myneni, R.B.; Sitch, S.; Friedlingstein, P.; Cramer, W.; Bousquet, P.; Buermann, W.; Smith, B. Climatic control of the high-latitude vegetation greening trend and Pinatubo effect. *Science* **2002**, *296*, 1687–1689. [CrossRef] [PubMed]